International Journal of Biological Macromolecules 371 (2026) 152961

Contents lists available at ScienceDirect

International Journal of Biological Macromolecules

journal homepage: www.elsevier.com/locate/ijbiomac

Nanoparticle-based delivery of corn silk extract for the treatment of CCl_4-induced hepatotoxicity

Alyaa Farid [a,*], Aya Badawi [b], Malak Waheed [b], Mohamed Ashraf [a], Maryam Amr [a], Ayman Amin [c]

[a] Biotechnology Department, Faculty of Science, Cairo University, Giza, Egypt
[b] Faculty of Biotechnology, October University for Modern Sciences and Arts, Giza, Egypt
[c] Faculty of Agriculture, Cairo University, Giza, Egypt

ARTICLE INFO

Keywords:
Liver injury
Corn silk
Chitosan

ABSTRACT

Liver injury is a significant global health concern that requires effective therapeutic strategies. Corn silk is traditionally recognized for its health-promoting properties due to its rich content of bioactive compounds. This study aimed to develop corn silk extract-loaded chitosan nanoparticles (CSE-CSNPs) *via* ionic gelation and evaluate their hepatoprotective efficacy against CCl_4-induced liver injury in rats. CSE-CSNPs exhibited favorable physicochemical properties, including a mean size of 59.03 nm and a positive zeta potential of 45.61 mV, with encapsulation efficiency of 73.2% for total phenolics. *In vitro* assays confirmed the biocompatibility and enhanced antioxidant activity of the nanoformulation. *In vivo*, treatment with CSE-CSNPs (100 mg/kg/day) for four weeks significantly ameliorated CCl_4-induced liver injury. Serum ALT levels decreased from 84.2 U/L in untreated CCl_4 rats to 49.2 U/L in CSE-CSNPs-treated rats, approaching the control value of 50.6 U/L. Similarly, AST and ALP were reduced from 101.0 U/L and 149.6 U/L to 70.6 U/L and 109.6 U/L, respectively. Oxidative stress markers showed comparable restoration, with hepatic MDA decreasing from 24.0 to 10.6 ng/mg protein, while GSH, SOD, and CAT increased from 55.4 μg/mg protein, 31.2 U/mg protein, and 22.2 U/mg protein to 97.6 μg/mg protein, 55.2 U/mg protein, and 63.4 U/mg protein, respectively- all values comparable to healthy controls. Notably, the nanoformulation achieved superior hepatoprotection at half the dose of free corn silk extract, demonstrating enhanced bioavailability and therapeutic efficacy. These findings highlight the potential of chitosan nanoparticle-mediated delivery as a promising strategy to improve the hepatoprotective activity of corn silk extract.

List of materials

- 1,1-diphenyl-2-picryl hydrazyl (DPPH) (Sigma-Aldrich, USA)
- 3-(4,5-dimethylthiazol-2-yl)-2-5-diphenyltetrazolium bromide (MTT) (Sigma-Aldrich, USA)
- Acetic acid
- $AlCl_3$
- Azinobistetrazolium sulfate (ABTS)
- Carbon tetrachloride (CCL4)
- CH_3COOK
- Chitosan (low M.Wt. (50,000–190,000 Da based on viscosity, ≥75% deacetylated) (Sigma-Aldrich, USA)
- Chloroform
- Cold Tris–HCl buffer
- Deionized water
- Dimethyl sulfoxide (DMSO) (Sigma-Aldrich, USA)
- Distilled water
- Ethanol (85%)
- $FeCl_3$
- Ferric ion reducing antioxidant power (FRAP)
- Folin-Ciocalteu reagent
- H_2SO_4
- HCl
- Heparin
- HNO_3
- Indomethacin (Sigma-Aldrich, USA)
- Methyl alcohol
- Na_2CO

* Corresponding author.
E-mail address: alyaafarid@cu.edu.eg (A. Farid).

https://doi.org/10.1016/j.ijbiomac.2026.152961
Received 26 March 2025; Received in revised form 18 April 2026; Accepted 7 June 2026
Available online 8 June 2026

Abbreviations

1, 1-diphenyl-2-picryl hydrazyl DPPH
2,4,6-Tri(2-pyridyl)-*s*-triazine TPTZ
3-(4,5-dimethylthiazol-2-yl)-2-5-diphenyltetrazolium bromide MTT
Alkaline phosphatase ALP
Aspartate aminotransferase AST
Azinobistetrazolium sulfate cation ABTS+
Carbon tetrachloride CCL4
Catalase CAT
Dimethyl sulfoxide DMSO
Direct bilirubin DB
Drug-induced liver injury DILI
Dynamic light scattering DLS
Ferric ion reducing antioxidant power FRAP
Gas chromatography-mass spectroscopy GC–MS
Glutathione GSH
Hyaluronic acid HA
Inductively coupled plasma optical emission spectroscopy ICP-OES
Interleukin IL
Laminin LN
Malondialdehyde MDA
Matrix metalloproteinases MMP
Nanoparticles NPs
One way analysis of variance ANOVA
Partial thromboplastin time PTT
Polytetrafluoroethylene PTFE
Prothrombin time PT
Red blood cells RBCs
Roussel Uclaf Causality Assessment Method RUCAM
Rutin equivalent RE
Sodium tripolyphosphate TPP
Superoxide dismutase SOD
Theodor Bilharz Research Institute TBRI
Tissue inhibitor of metalloproteinases TIMP
Total bilirubin TB
Transmission electron microscope TEM
Tumor necrosis factor TNF- α
Type 4 collagen IV-C
Type III procollagen PCIII

- Partial thromboplastin time (PTT) and prothrombin time (PT) reagents (Thermo Fisher Scientific, USA)
- Phosphate buffered saline
- Potassium persulfate
- Rat's ALP ELISA kit (MBS011598, MyBioSource, USA)
- Rat's ALT ELISA kit (MBS264975, MyBioSource, USA)
- Rat's AST ELISA kit (MBS269614, MyBioSource, USA)
- Rat's Bax ELISA kit (MBS935667, MyBioSource, USA)
- Rat's Bcl2 ELISA kit (MBS2515143, MyBioSource, USA)
- Rat's caspase 3 ELISA kit (MBS018987, MyBioSource, USA)
- Rat's caspase 8 ELISA kit (MBS260539, MyBioSource, USA)
- Rat's CAT ELISA kit (MBS006963, MyBioSource, USA)
- Rat's DB ELISA kit (MBS9389077, MyBioSource, USA)
- Rat's GSH ELISA kit (MBS265966, MyBioSource, USA)
- Rat's HA ELISA kit (MBS727090, MyBioSource, USA)
- Rat's IL-10 ELISA kit (MBS2707969, MyBioSource, USA)
- Rat's IL-17 ELISA kit (MBS2022678, MyBioSource, USA)
- Rat's IL-18 ELISA kit (MBS260091, MyBioSource, USA)
- Rat's IL-1β ELISA kit (MBS764668, MyBioSource, USA)
- Rat's IV-C ELISA kit (MBS732756, MyBioSource, USA)
- Rat's LN ELISA kit (MBS453848, MyBioSource, USA)
- Rat's MDA ELISA kit (MBS738685, MyBioSource, USA)
- Rat's MMP9 ELISA kit (*E*-EL-R3021, ElabScience, USA)
- Rat's p53 ELISA kit (MBS723886, MyBioSource, USA)
- Rat's PCIII ELISA kit (MBS705525, MyBioSource, USA)
- Rat's SOD ELISA kit (MBS036924, MyBioSource, USA)
- Rat's TB ELISA kit (MBS730053, MyBioSource, USA)
- Rat's TIMP1 ELISA kit (*E*-EL-R0540, ElabScience, USA)
- Rat's TNF-α ELISA kit (MBS267737, MyBioSource, USA)
- RPMI media (Sigma-Aldrich, USA)
- Sodium hydroxide
- Sodium pentobarbital (Sigma-Aldrich, USA)
- Sodium Tripolyphosphate (Sigma-Aldrich, USA)
- Tri(2-pyridyl)-*s*-triazine) (TPTZ)
- William's complete medium

1. Introduction

Drug-induced liver injury (DILI) is a predominant adverse effect associated with many medications, as the liver serves as the primary site for drug metabolism. Clinical consequences range from drug withdrawal in mild cases to hospitalization or even liver transplantation in severe cases [1]. It is the most frequent cause of acute liver injury in the United States [2]. Pharmaceuticals can induce liver damage through direct toxicity of the drug or its metabolites, immune-mediated injury, or exacerbated toxicity from subsequent inflammatory responses [3]. Notably, several herbal treatments, including yaqona, Mormon-tea, Scutellaria, *Mentha pulegium*, and ashwagandha, have also been implicated in acute liver injury [4].

Many lipophilic drugs are metabolized in the liver *via* phase I reactions involving the cytochrome P450 system [5], generating reactive intermediates that can damage cellular organelles such as mitochondria, leading to hepatocyte dysfunction and injury [6]. These harmful intermediates are normally neutralized during phase II conjugation reactions (*e.g.*, with glucuronate, glutathione, or sulfate). Hepatotoxicity occurs when the production of phase I metabolites exceeds the liver's detoxification capacity or when conjugating agents are depleted, resulting in metabolite accumulation. A key early event in DILI is the disruption of the mitochondrial respiratory chain, which increases reactive oxygen species (ROS) production and depletes adenosine triphosphate (ATP), ultimately triggering hepatocyte death [7]. This often occurs *via* necrosis, amplifying the hepatic inflammatory cascade [8]. The liver houses both innate and adaptive immune cells [9], where inflammatory responses play a major role in hepatotoxicity. Drug metabolites may bind to cellular proteins and be presented on major histocompatibility complex (MHC) molecules to T lymphocytes, creating an environment characterized by inflammatory cytokine accumulation and ROS production that leads to hepatocyte death [10]. When DILI is suspected, discontinuation of non-essential medications is recommended [11,12], often leading to improved liver function tests as assessed by the Roussel Uclaf Causality Assessment Method (RUCAM) criteria [13,14]. Although liver damage resolves completely in most cases, some patients develop persistent injury, liver failure requiring transplantation, or mortality. Despite substantial advances in understanding the clinical and mechanistic aspects of DILI, effective therapeutic strategies remain limited and require further investigation [15].

Plant-derived antioxidants, particularly phytophenolics, have gained attention for their potential to reduce drug-induced liver damage [16–18]. Their hepatoprotective effects are primarily attributed to neutralizing free radicals, thereby protecting cellular membranes and macromolecules from ROS-mediated injury. Additionally, these natural products modulate cytochrome P450 isoforms, enhance antioxidant enzyme synthesis, elevate phase II enzyme levels, and inhibit toxin uptake [18]. Several natural compounds with considerable efficacy, low

toxicity, and high availability, such as silymarin, resveratrol, curcumin, and ginkgo, have been investigated for their hepatoprotective properties [16–18].

Corn (*Zea mays* L.) is one of the world's most cultivated crops, with its grains, leaves, silk, stalk, and inflorescence traditionally used as remedies for various ailments. Corn silk (Maydis stigma)—the elongated, soft, yellowish fibers found within corn husks—has been utilized in herbal therapy for its diuretic, antilithic, uricosuric, and antibacterial properties, with applications in treating edema, urinary tract infections, arthritis, kidney stones, nephritis, and prostatitis [19,20]. Although considered an agricultural by-product often discarded or used as animal feed [21], corn silk is rich in carbohydrates, protein, vitamins, minerals, fibers, and flavonoids with well-documented antioxidant properties [22–25]. These bioactive compounds are associated with the prevention of chronic inflammatory conditions [26–28], and numerous *in vivo* and clinical studies have confirmed their safety for human consumption [29]. Consequently, corn silk is increasingly incorporated into value-added food products, and prior research has highlighted its abundant phenolic and flavonoid content, as well as the antioxidant activity of its polysaccharides [30,31].

Despite the well-documented hepatoprotective properties of corn silk extract (CSE) [19–31], its clinical translation has been limited by inherent drawbacks common to many plant-derived compounds [32–34] such as poor aqueous solubility, low oral bioavailability, rapid metabolic degradation, and lack of targeted delivery [35]. To address these limitations, this study introduces a novel therapeutic approach by encapsulating CSE within chitosan nanoparticles (CSNPs). Chitosan, a biodegradable and mucoadhesive cationic polymer, offers distinct advantages for oral delivery, including enhanced intestinal absorption, prolonged gastrointestinal retention, and controlled release of encapsulated bioactives [36–42]. While chitosan nanoparticles have been extensively employed as carriers for various therapeutic agents, their application for the nanoencapsulation of CSE, specifically for hepatoprotection, has not yet been explored. This study, therefore, represents the first investigation to develop and evaluate CSE-loaded chitosan nanoparticles (CSE-CSNPs) for the management of DILI.

This study advances beyond the existing literature in several key respects. The nanoformulation was comprehensively characterized for physicochemical properties, encapsulation efficiency, and release kinetics under simulated gastrointestinal conditions, parameters critical for oral delivery but rarely reported together for herbal extracts. The therapeutic efficacy is systematically evaluated through a multi-

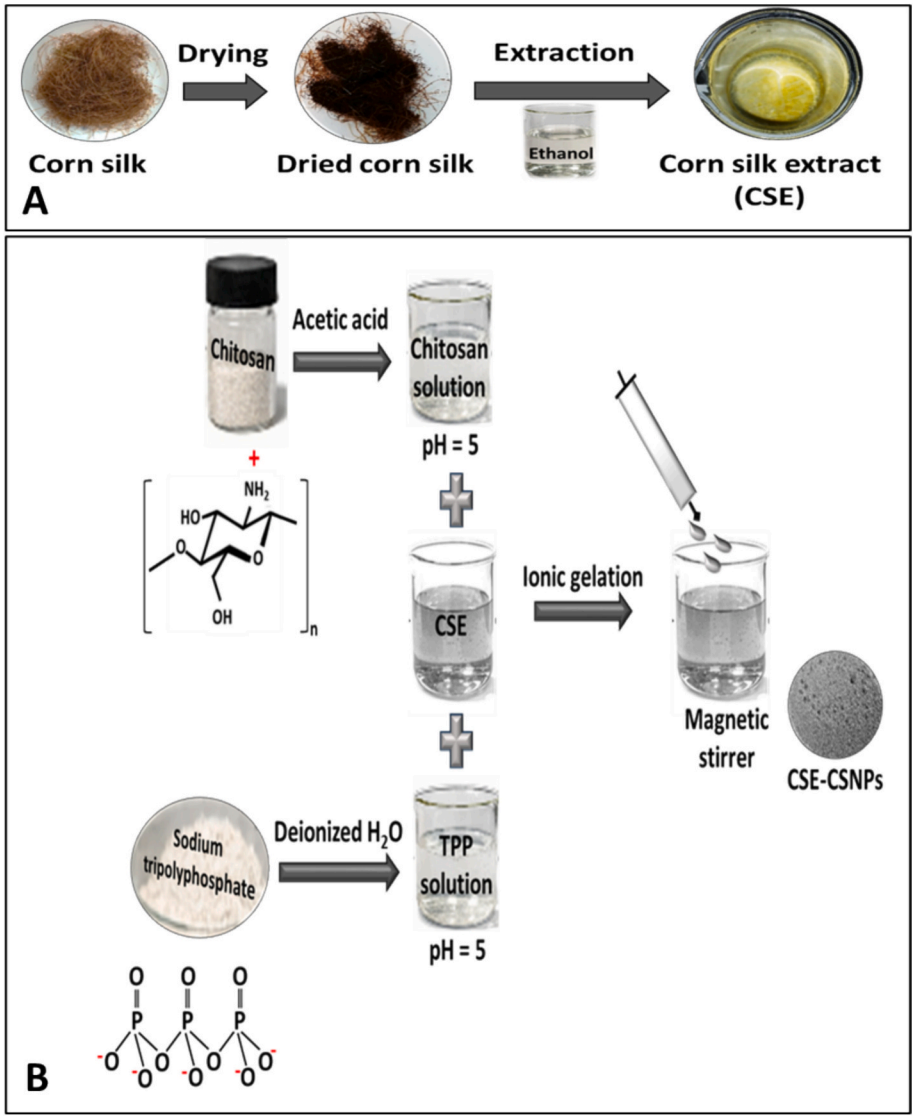

Fig. 1. Schematic representation of A] Preparation of CSE: corn silk was dried at 50 °C until constant weight, ground into powder, and extracted with 70% ethanol (1:10 w/v) for 48 h; and B] Preparation of CSE-CSNPs *via* ionic gelation method: chitosan solution (pH 5.0) was mixed with sodium tripolyphosphate (TPP) and CSE, resulting in electrostatic cross-linking and formation of CSE-CSNPs. Created using Microsoft PowerPoint.

parametric *in vivo* approach encompassing liver function, oxidative stress, inflammation, apoptosis, and tissue remodeling, addressing the multifaceted pathology of DILI more comprehensively than prior studies that focused on individual pathways. Critically, CSE-CSNPs achieve superior hepatoprotection at half the dose of free CSE, establishing proof-of-concept that chitosan nanoencapsulation significantly enhances the bioavailability and therapeutic potency of corn silk bioactives. Collectively, these findings position CSE-CSNPs as a promising nanotherapeutic strategy that bridges traditional herbal medicine with modern drug delivery technology.

2. Materials and methods

2.1. Collection and extraction of corn silk

Corn silk (*Zea mays* L.) was collected at the silking stage from the agriculture farm of Cairo University, Egypt. The samples were washed, blanched at 100 °C for 1 min, dried at 50 °C until constant weight, ground into powder, and sieved through a 22-mesh sieve [43]. The dried corn silk powder was incubated in ethyl alcohol (1:10 *w/v*) for 48 h (Fig. 1A). The extract was filtered, evaporated under vacuum, and stored at −20 °C until use [29]. Detailed procedures for collection and extraction are provided in supplementary materials.

2.2. Preparation of CSE-CSNPs

CSE-CSNPs was prepared by the ionic gelation technique, which entailed the combination of sodium tripolyphosphate (TPP) anions with chitosan cations (Fig. 1B). Chitosan (medium molecular weight, Sigma-Aldrich, USA) solution (50 mL) was prepared at a concentration of 1.5 mg/mL by dissolving it in an aqueous solution of acetic acid (0.5 mL acetic acid completed to 50 mL by water). NaOH was used to adjust the pH of the solution to 5; and the chitosan solution was stirred using a magnetic stirrer at room temperature until the complete dissolving of chitosan. TPP (Sigma-Aldrich, USA) was added to deionized water (20 mL) and stirred for half an hour until complete dissolving to form TPP solution at a concentration of 0.7 mg/mL, with pH adjusted to 5 using HCl (0.1 M). The TPP solution was added to the chitosan solution while maintaining continuous stirring until the stabilization of CSNPs was achieved. For preparation of CSE-CSNPs, TPP solution was mixed with CSE at a concentration of 6 mg/mL, and the resulting mixture was subsequently added to chitosan solution to produce CSE-CSNPs. CSNPs and CSE-CSNPs were lyophilized and subsequently stored in the refrigerator. The size of the prepared NPs was determined using transmission electron microscopy (TEM). The zeta potential of CSNPs and CSE-CSNPs was measured using a Zetasizer (Malvern Instruments). The hydrodynamic size of the prepared NPs was determined using the dynamic light scattering (DLS) technique.

2.3. Determination of encapsulation efficiency (EE%) and drug loading (DL%)

The EE% and DL% of CSE-CSNPs were determined using quantification methods based on the total TPC and TFC of the extract. A precisely measured volume (2 mL) of the freshly prepared CSE-CSNPs suspension was transferred to an Amicon® Ultra centrifugal filter unit. The unit was centrifuged at 20,000 ×*g* for 45 min at 4 °C to separate the NPs pellet from the aqueous supernatant containing unencapsulated (free) CSE compounds. The clear filtrate was carefully collected for analysis of free compounds.

The TPC and TFC of the filtrate were immediately analyzed to determine the amount of unencapsulated extract. TPC was determined using the Folin-Ciocalteu method, with results expressed as Gallic Acid Equivalents (GAE). TFC was determined *via* the aluminum chloride colorimetric method, with results expressed as Quercetin Equivalents (QE). These values represented the free (unencapsulated) TPC and TFC. The amount of encapsulated compounds was calculated by subtracting the amount of free compounds from the total amount used in the formulation batch. EE% was then calculated separately for phenolics and flavonoids using the following equations: EE% (TPC) = [(Total TPC added to formulation) − (Free TPC in filtrate)] / (Total TPC added to formulation) × 100 or EE% (TFC) = [(Total TFC added to formulation) − (Free TFC in filtrate)] / (Total TFC added to formulation) × 100, where "Total TPC/TFC added" is the known phenolic/flavonoid content of the precise amount of crude CSE used to prepare the nanoparticle batch.

The nanoparticle pellet retained in the Amicon filter unit was washed three times with cold deionized water to remove any adsorbed surface compounds. The washed pellet was then resuspended in a minimal volume of water, frozen at −80 °C, and lyophilized to obtain the dry mass of the nanoparticles (CSNPs + encapsulated extract). The exact weight of the lyophilized powder was recorded. DL% was determined as [(TPC/TFC in CSE-CSNPs)/(Total weight of NPs)] × 100. All analyses for EE% and DL% were performed in triplicate ($n = 3$) from independently prepared NPs batches. Results were expressed as mean ± standard deviation (SD).

2.4. In vitro release profile under simulated gastrointestinal conditions

The release kinetics of the encapsulated CSE from chitosan nanoparticles were evaluated under simulated gastrointestinal (GI) conditions using a sequential pH-change model to mimic gastric and intestinal transit.

2.4.1. Preparation of simulated gastrointestinal fluids

Simulated fluids were prepared fresh on the day of the experiment. Simulated gastric fluid (SGF), pH 1.2, was prepared by dissolving 2.0 g of sodium chloride (NaCl) and 3.2 g of pepsin in 800 mL of deionized water. The pH was adjusted to 1.2 using concentrated hydrochloric acid (HCl, 37%), and the final volume was completed to 1000 mL. The solution was equilibrated to 37 °C before use. Simulated intestinal fluid (SIF), pH 6.8, was prepared by dissolving 6.8 g of monobasic potassium phosphate (KH_2PO_4) in 750 mL of deionized water. The pH was adjusted to 6.8 using 0.2 M sodium hydroxide (NaOH) solution. Then, 10.0 g of pancreatin was added, and the mixture was gently stirred until dissolved. The final volume was adjusted to 1000 mL with deionized water and equilibrated to 37 °C.

2.4.2. Release study

The study was conducted using the dialysis bag diffusion method under sink conditions. A volume of the nanoparticles suspension was placed into a pre-hydrated dialysis bag (cellulose membrane, molecular weight: 12–14 kDa). The bag was securely sealed and immersed in 200 mL of pre-warmed (37 °C) SGF contained in a glass vessel for 2 h. After 2 h, the dialysis bag was carefully transferred to a fresh vessel containing 200 mL of pre-warmed SIF (pH 6.8). The release study was continued for an additional 22 h. The system was maintained at 37 °C in a thermostatically controlled shaking water bath operating at 100 rpm to simulate GI motility.

At predetermined time intervals (0.5, 1, 1.5, 2, 3, 4, 6, 8, 12, and 24 h), 2 mL aliquots were withdrawn from the external release medium (the SGF or SIF surrounding the dialysis bag). An equal volume (2 mL) of the corresponding fresh, pre-warmed release medium was immediately replenished to maintain a constant volume and sink conditions. The collected samples were filtered through a 0.22 μm syringe filter. The concentration of the released CSE in each sample was quantified by measuring the TPC.

2.5. Nutritional and mineral composition of corn silk

The nutritional composition (moisture, protein, fat, crude fiber, ash, and carbohydrates) of corn silk powder was analyzed using standard

AOAC methods [44–47]. Mineral composition (Ca, Cu, Fe, K, Mg, Mn, Na, and Zn) was determined by inductively coupled plasma optical emission spectroscopy (ICP-OES) following microwave digestion [25]. Detailed procedures are provided in supplementary materials.

2.6. Phytochemical screening

Qualitative phytochemical screening for primary and secondary metabolites (phenols, flavonoids, tannins, terpenoids, alkaloids, cardiac glycosides, sterols, phlobatannins, and proteins) was performed using standard colorimetric methods [48–50]. Details of the assays are provided in supplementary materials.

2.7. Determination of total phenolic content (TPC) and total flavonoid content (TFC)

TPC was determined using the Folin-Ciocalteu method and expressed as gallic acid equivalents (GAE) per gram of sample [51]. TFC was determined by the aluminum chloride colorimetric method and expressed as quercetin equivalents (QE) per gram of sample [43]. Detailed procedures are provided in supplementary materials.

2.8. Gas chromatography-mass spectroscopy (GC–MS) analysis of CSE and CSE-CSNPs

Bioactive compounds in CSE and CSE-CSNPs were identified using GC–MS on an Rtx-5MS fused capillary column, with compound identification based on retention time and mass spectral matching [52].

2.9. In vitro examination of NPs

For all *in vitro* testing, the doses of CSE-CSNPs were based on the actual amount of encapsulated extract, as determined by the DL of 16.64% (*w*/w) [encapsulated extract (μg/mL) = NPs concentration (μg/mL) × DL%].

2.9.1. Free radical scavenging capacity

To evaluate the free radical scavenging capacity, CSE, CSNPs, and CSE-CSNPs were analyzed against various types of free radicals: DPPH (2, 2-diphenyl-1-picryl-hydrazyl), ABTS+ (azinobistetrazolium sulfate cation), and FRAP (ferric ion reducing antioxidant power). The inhibition % was calculated using the formula: [1 - (sample absorbance / control absorbance)] X 100.

2.9.1.1. DPPH assay. The antioxidant activities of the CSE, CSNPs, and CSE-CSNPs were estimated by the DPPH free radical scavenging activity [53] (Fig. 2A). 0.2 mL of sample was completed to 1 mL using methanol; followed by the addition of 4 mL of freshly prepared DPPH methanolic solution (0.2 mM). The solution was kept in the dark for 30 min. The absorbance was read at 517 nm.

2.9.1.2. ABTS assay. ABTS + cation radical was obtained from the mixing of ABTS (7 mM, in water) and potassium persulfate 2.45 mM, at a ratio of 1:1, and incubated for 16 h at room temperature in the dark. The

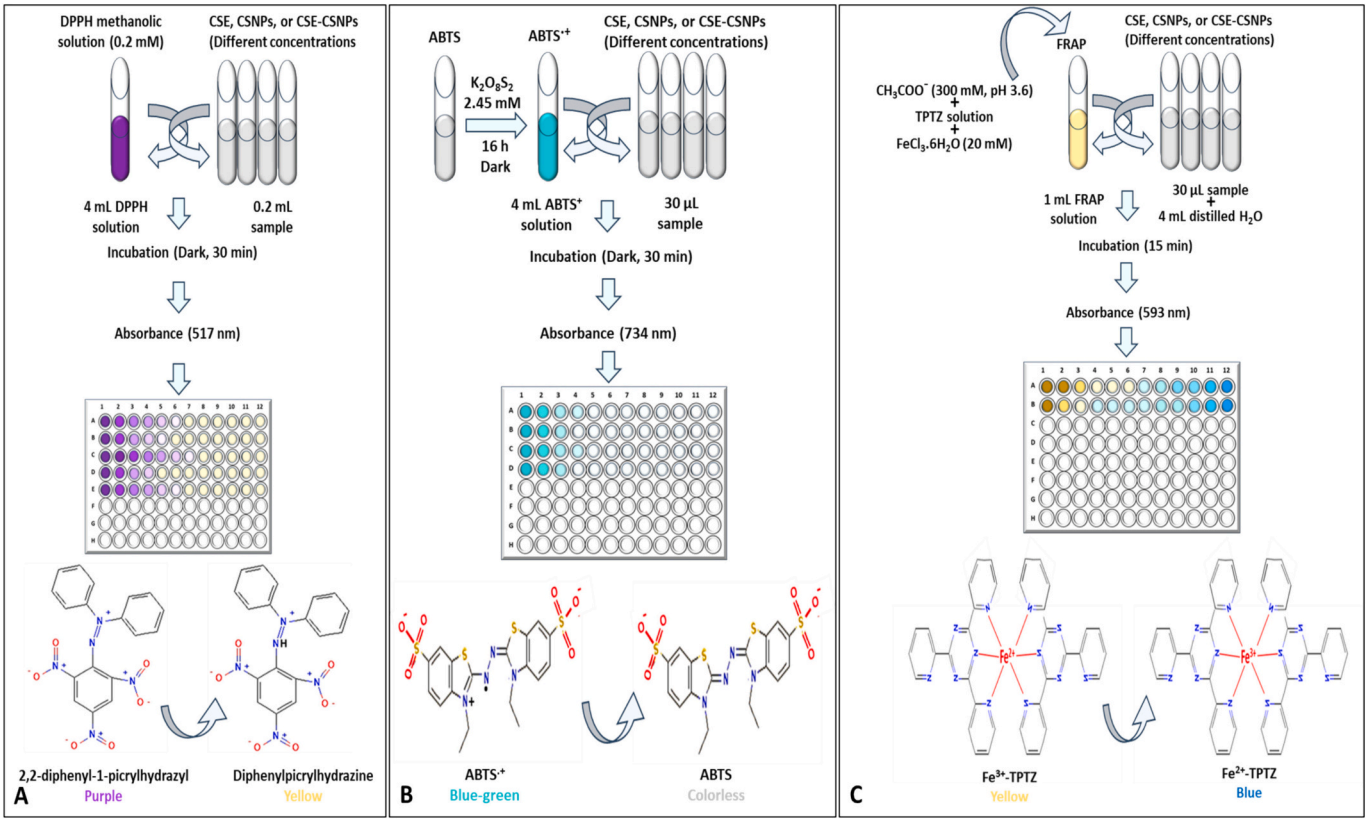

Fig. 2. Schematic representation of antioxidant assays used to evaluate CSE, CSNPs, and CSE-CSNPs. A] DPPH assay: DPPH methanolic solution (purple) is reduced by antioxidants to a yellow-colored product. The reaction mixture is incubated for 30 min in the dark, and absorbance is measured at 517 nm; B] ABTS assay: ABTS is mixed with potassium persulfate and incubated for 16 h in the dark to generate the blue-green $ABTS^{+}$ radical. Upon reaction with antioxidants, the radical is reduced to a colorless product. After 5 min incubation, absorbance is measured at 734 nm; and C] FRAP assay: The FRAP working solution (containing acetate buffer, TPTZ, and $FeCl_3$) is pale yellow. In the presence of antioxidants, Fe^{3+} is reduced to Fe^{2+}, forming an intense blue-colored complex. After 15 min incubation, absorbance is measured at 593 nm. Created using Microsoft PowerPoint. Chemical structures of DPPH, ABTS, and TPTZ used in schematic figures were retrieved from the PubChem database (https://pubchem.ncbi.nlm.nih.gov). PubChem is a public database maintained by the National Center for Biotechnology Information (NCBI), National Library of Medicine, National Institutes of Health (NIH), USA.

absorbance (at 734 nm) of 0.700 was obtained by diluting the ABTS + solution with 80% ethyl alcohol. 30 μL of sample were mixed with ABTS + solution (4 mL) and completed to 1 mL using distilled water; and the mixture was incubated for 5 min followed by measuring the absorbance [29] (Fig. 2B).

2.9.1.3. Ferric ion reducing antioxidant power (FRAP). Twenty five mL of acetate buffer (300 mM, pH 3.6) was mixed with 2.5 mL of TPTZ (2,4,6-Tri(2-pyridyl)-*s*-triazine) solution and 2.5 mL of ferric chloride hexahydrate solution (20 mM) followed by incubation at 37 °C. Different concentrations of the sample (30 μL) were completed to 4 mL with distilled water then mixed with the working solution (1 mL). After 15 min incubation, absorbance was determined at 593 nm [54] (Fig. 2C).

2.9.2. Cytotoxicity (MTT) assay

The method of Shen et al. [55] was used for the preparation of hepatocyte cell cultures under sterile conditions (Fig. 3A). Rats were anesthetized with 50 mg/kg sodium pentobarbital and perfused by collagenase buffer through their portal vein. The liver was cut open to separate the cells after perfusion, which then suspended in William's complete medium, passed through a nylon filter with a mesh size of 100 μm. 100 μL of 10^5 hepatocytes were cultured, at 37 °C for 24 h, to develop the cells monolayers. After incubation, monolayers were washed 3 times. CSE, CSNPs or CSE-CSNPs at different concentrations were added to the culture medium (RPMI) that was introduced to the cells followed by 24 h of incubation. 20 μL of MTT [3-(4,5-dimethylthiazol-2-yl)-2–5-diphenyltetrazolium bromide] at a concentration of 5 mg/mL were introduced to the cultured cells followed by 4 h of incubation at 37 °C and 5% CO_2. Dimethyl sulfoxide (DMSO) was added to the plates and the absorbance was read at 560 nm.

2.9.3. Estimation of the anti-inflammatory activity

Heparinized fresh rat blood (5 mL) was centrifuged for red blood cells (RBCs) preparation for 15 min at 1200 rpm (Fig. 3B). After discarding the supernatant, the produced pellet was dissolved using an isotonic buffer (phosphate buffered saline). In various concentrations, CSE, CSNPs and CSE-CSNPs were mixed with 3 mL of distilled water (hypotonic solution) or phosphate buffered saline (isotonic solution). The control consisted of 3 mL of indomethacin (200 mg/mL). RBCs' suspension (0.1 mL) was added to CSE, CSNPs or CSE-CSNPs and incubated for 60 min followed by centrifugation for 15 min at 1200 rpm. The quantity of released hemoglobin was determined at 540 nm.

2.9.4. Estimation of the anticoagulant activity

The prothrombin time (PT) and partial thromboplastin time (PTT) were used to determine the coagulant activities of CSE, CSNPs and CSE-CSNPs (Fig. 3C). Different concentrations of the samples were combined with 900 μL of rat's plasma. The clotting time in seconds was measured, at 37 °C, and compared to that of heparin.

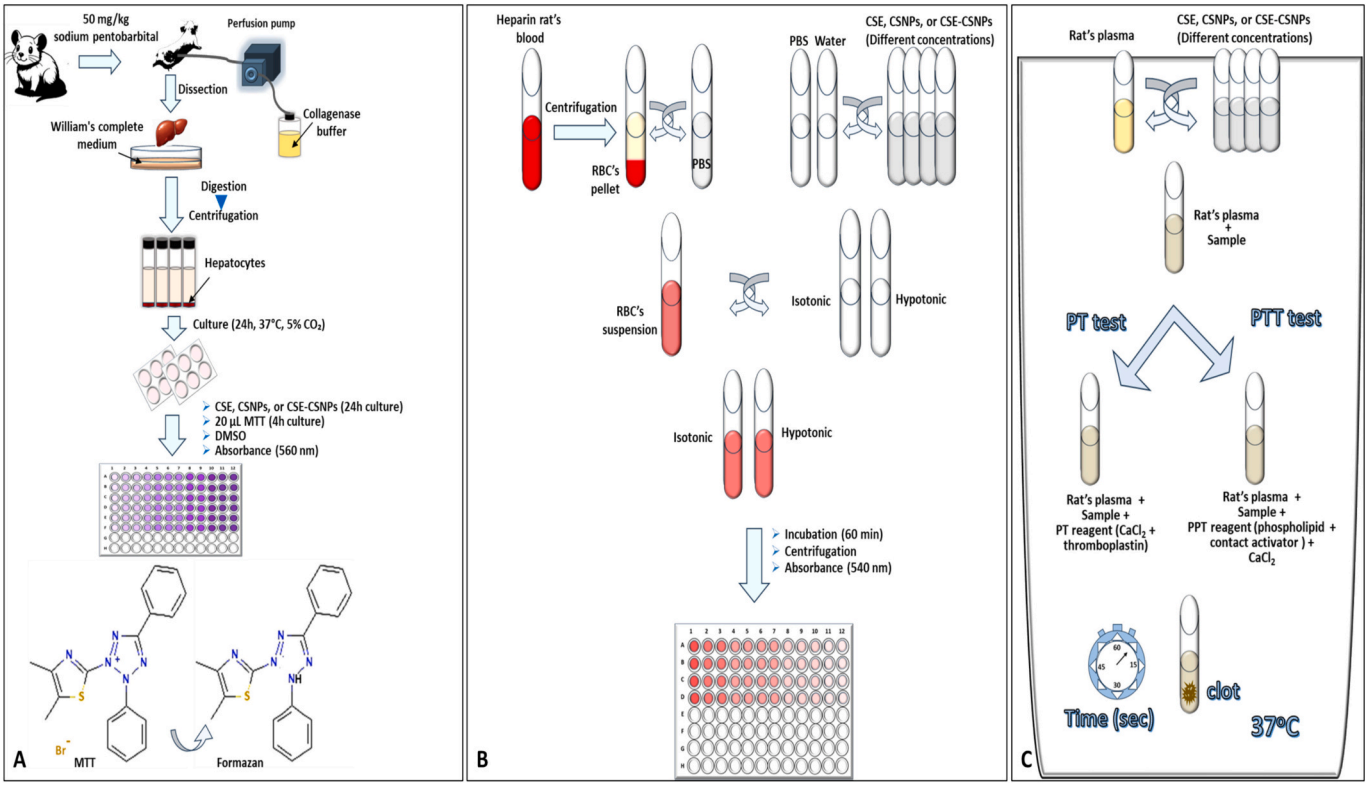

Fig. 3. Schematic representation of cytotoxicity, anti-inflammatory, and anticoagulant assays used to evaluate CSE, CSNPs, and CSE-CSNPs. A] MTT assay: rat hepatocytes are cultured in a plate and treated with test samples. MTT (yellow) is added and reduced by mitochondrial enzymes of viable cells to purple formazan crystals. DMSO is added to dissolve the crystals, and absorbance is measured at 560 nm. Higher absorbance indicates greater cell viability; B] Hemolysis inhibition assay (anti-inflammatory): Rat RBCs are exposed to hypotonic solution in the presence or absence of test samples. RBC membrane stabilization is indicated by reduced hemoglobin release (clear or pale colour), while hemolysis is indicated by pink/red colour. Absorbance is measured at 540 nm; and C] Anticoagulant assays (PT and PTT): Rat plasma is incubated with test samples. For PT assay, PT reagent (thromboplastin and calcium) is added, and time to clot formation is recorded. For PTT assay, PTT reagent (phospholipid and contact activator) is added, incubated for 3–5 min, then calcium chloride is added, and time to clot formation is recorded. Clot formation is detected by the appearance of fibrin strands or a gel-like mass that does not flow when the tube is tilted. Created using Microsoft PowerPoint. Chemical structures of MTT used in schematic figure were retrieved from the PubChem database (https://pubchem.ncbi.nlm.nih.gov). PubChem is a public database maintained by the National Center for Biotechnology Information (NCBI), National Library of Medicine, National Institutes of Health (NIH), USA.

2.10. In vivo examination

30 male Sprague Dawley rats (weighted 180 g and aged 8 weeks old) were obtained from Theodor Bilharz Research Institute (TBRI) and divided into 6 groups (5 rats/ group) (Fig. 4); Group I: healthy control rats, group II: healthy vehicle group that received olive oil (0.1 mL) twice/week for three successive weeks by intraperitoneal (i.p) injection, group III: untreated rats that received CCl_4 50% (*v*/v) dissolved in olive oil at a volume of 0.4 mL/kg twice/week for three successive weeks by i.p injection, group IV: rats with CCl_4-induced liver injury that received CSE (200 mg/kg/day) by oral gavage for four weeks, group V: rats with CCl_4-induced liver injury that received unloaded-CSNPs (100 mg/kg/day) by oral gavage for four weeks and group VI: rats with CCl_4-induced liver injury that received CSE-CSNPs (100 mg/kg/day) by oral gavage for four weeks. The dose of CSE-CSNPs (100 mg/kg/day) was selected based on a dual rationale. First, it delivers a substoichiometric payload of the active CSE compared to the free CSE group (200 mg CSE/kg). This design provides a direct test of whether nanoencapsulation enhances bioavailability and efficacy. Second, this dose aligns with the established, well-tolerated range (50–100 mg/kg) for orally administered CSNPs systems in rodent disease models, as demonstrated in prior studies [56–58]. All experimental procedures were carried out in accordance with the international guidelines for the care and use of laboratory animals and complied with the ARRIVE guidelines. The study was approved by the ethics committee of October University for Modern Sciences and Arts. Rats were given sodium pentobarbital (50 mg/kg) to induce terminal anesthesia at the end of the experiment. Cardiac puncture procedures were used for collecting blood samples from all groups. After clotting of blood samples at room temperature, serum was separated after centrifugation at 2000 rpm for 10 min and split into aliquotes to be stored at −80 °C. Animals were dissected to obtain their liver, then 1 g of liver specimens from each experimental group was homogenized utilizing cold Tris–HCl buffer to create liver tissue homogenate (10%).

2.10.1. Liver function evaluation

Liver function was measured using rat ELISA kits to measure levels of aspartate aminotransferase (AST), alanine aminotransferase (ALT), alkaline phosphatase (ALP), total bilirubin (TB), and direct bilirubin (DB) in serum samples (MBS269614, MBS264975, MBS011598, MBS730053, MBS9389077, MyBioSource, USA; respectively). Serum levels of laminin (LN), hyaluronic acid (HA), type III procollagen (PCIII), and type 4 collagen (IV-C) were also measured to evaluate liver fibrosis, using rat ELISA kits (MBS453848, MBS727090, MBS705525, MBS732756, MyBioSource, USA; respectively).

2.10.2. Oxidative stress markers

Lipid peroxidation marker in liver tissue was determined by measuring malondialdehyde (MDA) level; and the antioxidant effect was evaluated by determining superoxide dismutase (SOD), glutathione (GSH) and catalase (CAT) levels in liver tissue homogenates (MBS738685, MBS036924, MBS265966, MBS006963, MyBioSource, USA; respectively).

2.10.3. Inflammation evaluation

Inflammation was examined in liver tissue by measuring IL-10, IL-1β, IL-17, TNF-α, IL-18 levels (MBS2707969, MBS764668, MBS2022678, MBS267737 and MBS260091, MyBioSource, USA; respectively) by rat ELISA kits.

2.10.4. Liver tissue remodeling markers

The change in liver remodeling after treatment was conducted by detecting the levels of matrix metalloproteinases-9 (MMP9) (Rat ELISA kit, *E*-EL-R3021, Elabscience, USA) and tissue inhibitor of metalloproteinases-1 (TIMP1) (Rat ELISA kit, E-EL-R0540, Elabscience, USA).

2.10.5. Apoptosis evaluation

The effect of CSE, CSNPs and CSE-CSNPs on the levels of intracellular apoptotic proteins was utilized to evaluate apoptosis in liver. The anti-apopttotic protein Bcl2 (MBS2515143, MyBioSource, USA), and the

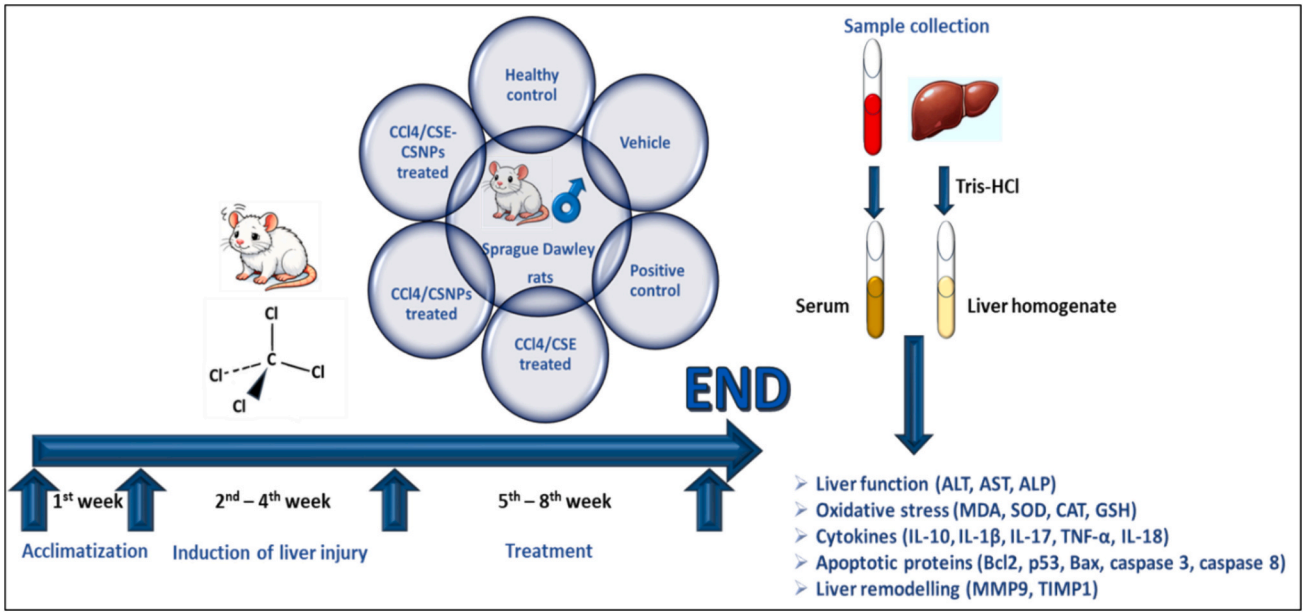

Fig. 4. Experimental design and animal grouping for the *in vivo* evaluation of CSE-CSNPs against CCl_4-induced liver injury in rats. Male Sprague Dawley rats ($n = 5$ per group) were divided into six groups: Group I (healthy control), Group II (vehicle control, olive oil), Group III (untreated CCl_4-induced liver injury, positive control), Group IV (CCl_4 + free CSE, 200 mg/kg/day), Group V (CCl_4 + unloaded CSNPs, 100 mg/kg/day), and Group VI (CCl_4 + CSE-CSNPs, 100 mg/kg/day). CCl_4 (50% *v*/v in olive oil, 0.4 mL/kg) was administered intraperitoneally twice weekly for three consecutive weeks. Treatments were administered orally by gavage daily for four weeks. At the end of the experiment, rats were euthanized; blood and liver tissues were collected for biochemical analyses. Created using Microsoft PowerPoint.

pro-apoptotic proteins (Bax, p53, caspase 3, and caspase 8) were measured in liver tissue homogenates by rat's ELISA kit, (MBS935667, MBS723886, MBS018987 and MBS260539, MyBioSource, USA; respectively)] [59].

2.11. Statistical analysis

Results were presented as mean ± SD and analyzed using one-way analysis of variance (ANOVA). Differences between means were assessed using Tukey's post-hoc test, with values considered significant when $P < 0.05$.

3. Results and discussion

3.1. Chemical analysis of corn silk

The chemical composition of CSE was characterized to confirm its bioactive potential prior to nanoencapsulation. Qualitative phytochemical screening revealed the presence of multiple bioactive classes, including phenols, flavonoids, alkaloids, and terpenoids (table S1). Nutritional and mineral analyses further demonstrated that the extract was rich in carbohydrates and contained essential macro- and micro-elements, particularly potassium, calcium, magnesium, and zinc (Table S1). Collectively, these results established CSE as a suitable candidate for nanoencapsulation.

The nutritional profile of our CSE aligned well with previous reports on corn silk. Aukkanit et al. [21] documented a similar composition of moisture, fats, ash, crude fiber, protein, and carbohydrates in corn silk powder. Likewise, the presence of essential minerals—potassium, calcium, and magnesium—has been consistently reported in corn silk beverages and dietary analyses [61,62]. These minerals are crucial for physiological functions, including blood pressure regulation and bone health [60]. Furthermore, the phytochemical classes identified in our extract (phenols, flavonoids, alkaloids, terpenoids, and cardiac glycosides) are well-established in the literature for their broad pharmacological potential, encompassing antioxidant, anti-inflammatory, antimicrobial, and cardioprotective activities [63–65].

Taken together, the comprehensive phytochemical and mineral profile of our CSE underscores its intrinsic bioactivity and provides a strong rationale for its selection as a candidate for development into an enhanced nanoformulation.

3.2. Physical characterization

In this study, CSE was loaded onto CSNPs using the ionic gelation method. This technique exploits electrostatic attraction between oppositely charged molecules; specifically, the cationic chitosan polymer and the anionic cross-linker sodium tripolyphosphate (TPP) [66–68]. Ionic gelation is favored for its simplicity, cost-effectiveness, and versatility, enabling efficient encapsulation of biomolecules with improved stability and controlled release profiles [69,70].

As a cationic polysaccharide, chitosan readily forms nanoparticles *via* this process. The resulting nanoparticles were characterized for size, morphology, and surface charge. TEM revealed that CSE-CSNPs possessed a uniform, spherical morphology with a size range of 49.61–51.12 nm (Fig. 5A). DLS analysis, which measures the hydrodynamic diameter in solution, showed an increase from 44.05 nm for blank CSNPs to 59.03 nm for CSE-CSNPs (Fig. 5B), confirming successful extract loading. Zeta potential measurements indicated a strong positive surface charge for both formulations (31.81 mV for blank CSNPs and 45.61 mV for CSE-CSNPs) (Fig. 5C).

These physicochemical parameters are critical determinants of nanoparticle performance *in vivo*. Particle size directly influences biodistribution, circulation time, and cellular uptake. Particles smaller than 100 nm, like those synthesized here, are optimal for avoiding rapid macrophage clearance and leveraging enhanced permeability and retention (EPR) effects [71–73]. The observed spherical morphology is advantageous due to its high surface area and reproducibility [74–76].

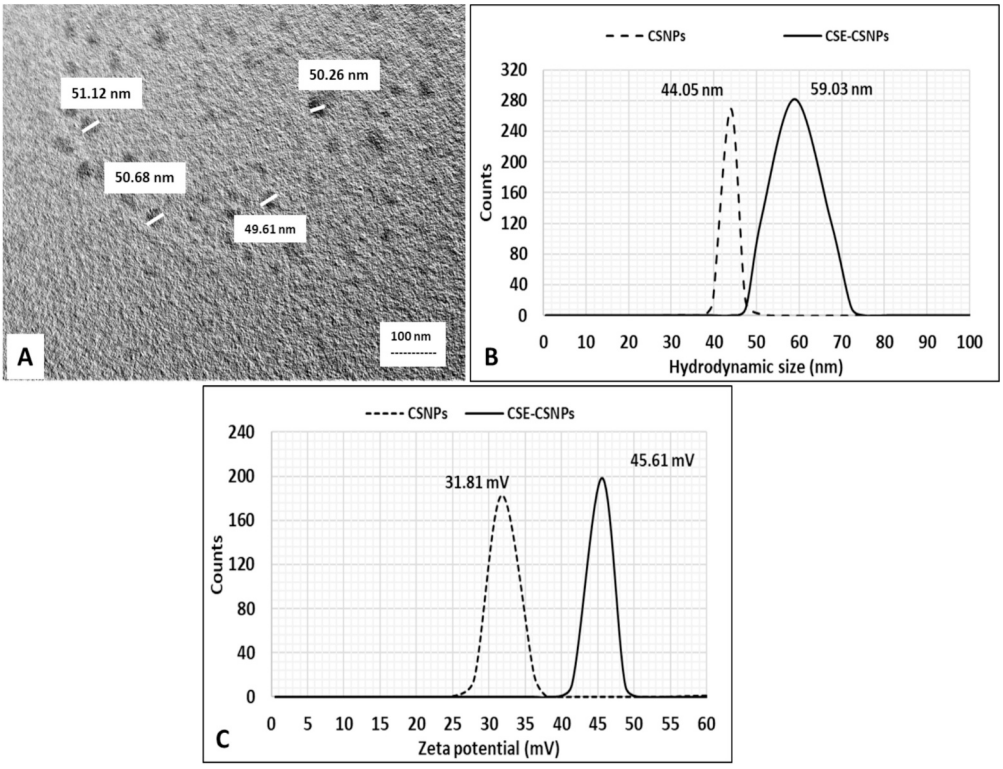

Fig. 5. Physical characterization of NPs showing A] TEM image of CSE-CSNPs; B] hydrodynamic size of CSNPs and CSE-CSNPs by DLS; and C] zeta potential of CSNPs and CSE-CSNPs.

Furthermore, the high positive zeta potential (> +30 mV) is a key indicator of colloidal stability, as strong electrostatic repulsion prevents particles aggregation during storage [77–79]. This cationic surface charge also promotes interaction with the anionic mucosal lining (rich in sialic and sulfonic acids), which can enhance mucoadhesion and residence time in the gastrointestinal tract following oral administration, thereby potentially improving bioavailability [80,81]. While an excessively high charge can sometimes limit passage through the gut lining, advanced formulations can refine this property to optimize both adhesion and absorption [82].

Collectively, the characteristics of CSE-CSNPs—small size, spherical shape, and high positive charge—support their suitability as an effective oral delivery system for the encapsulated phytochemicals. These favorable physicochemical properties provided a strong foundation for subsequent *in vitro* and *in vivo* evaluations.

3.3. EE% and DL% of CSE in CSNPs

The successful nanoencapsulation of CSE into CSNPs was quantitatively confirmed through EE% and DL% analyses based on the extract's TPC and TFC. The pure CSE exhibited high TPC (102.13 ± 2.93 mg GAE/g) and TFC (178.90 ± 3.51 mg QE/g), establishing a robust baseline of bioactive compounds for loading (Table 1). Following ultracentrifugation, the supernatant showed a substantial decrease in both TPC (27.23 mg GAE/g) and TFC (88.26 mg QE/g), indicating efficient entrapment of these phytochemicals within the nanoparticle matrix.

The calculated EE% was high for phenolics (73.2 ± 2.7%) and moderate for flavonoids (50.65 ± 0.83%). The strong EE% for phenolics aligned with the known affinity of chitosan (a cationic polysaccharide) for phenolic compounds, which can interact *via* hydrogen bonding, hydrophobic interactions, and ionic forces [83,84]. This interaction is a cornerstone of many successful polyphenol-loaded chitosan delivery systems [85]. The EE% for TFC, while lower, still represented significant flavonoid retention. This differential encapsulation is common in complex plant extracts, where the diverse physicochemical properties of individual compounds (*e.g.*, solubility, molecular size, and charge) lead to varied incorporation efficiencies.

The DL% capacity was notably high, with values of 16.64 ± 1.02% (TPC-based) and 20.14 ± 0.69% (TFC-based). The higher DL% based on TFC suggests a relative enrichment of flavonoids within the nanoparticle core. This phenomenon may be attributed to the stronger interaction of specific flavonoid structures with the chitosan polymer or to their preferential partitioning into the forming nanoparticle matrix during the ionic gelation process [86]. A high DL% is a critical attribute for therapeutic nanoparticles, as it reduces the amount of inert carrier material required to deliver an effective dose of the active compound, thereby improving efficacy and minimizing potential carrier-related side effects [87].

The combined metrics of high EE% and substantial DL% confirmed the successful development of an efficient nano-delivery system. These parameters are essential for ensuring adequate bioactive payload delivery, which directly translates to the enhanced *in vitro* and *in vivo* efficacy observed in this study [88]. The formulation's ability to efficiently load and retain key phenolic and flavonoid compounds of CSE provides a solid physicochemical foundation for its observed pharmacological superiority over the free extract.

3.4. In vitro release profile of CSE from CSE-CSNPs under simulated GI conditions

The *in vitro* release kinetics of CSE from CSE-CSNPs were evaluated under progressive simulated GI conditions to predict oral delivery behavior. The profile exhibited a biphasic pattern ideal for oral administration: an initial burst release during the gastric phase (simulated gastric fluid, SGF, pH 1.2), followed by sustained release in the intestinal phase (simulated intestinal fluid, SIF, pH 6.8) (Table 2). Approximately 32.33% of the payload was released within the first 2 h, with cumulative release reaching 84% after 24 h.

The initial burst release (19.33% within 0.5 h) is a common feature of polymeric nanoparticle systems and is primarily attributed to the rapid diffusion of CSE compounds adsorbed on or near the nanoparticle surface [89,90]. The acidic gastric environment (pH 1.2) also promotes protonation of chitosan's amino groups, enhancing polymer swelling and creating porous channels that facilitate the rapid efflux of superficially located drugs [91]. This early release can be advantageous for providing a rapid initial therapeutic effect following oral administration.

The subsequent sustained release phase in the intestinal medium (pH 6.8) is governed by a combination of diffusion and matrix erosion mechanisms. At near-neutral pH, chitosan chains deprotonate, reducing electrostatic repulsion and leading to a denser, more slowly degrading gel matrix [92]. The gradual degradation of this matrix *via* enzymatic or hydrolytic processes controls the sustained diffusion of the encapsulated core material over 24 h [93]. This sustained release profile is critical for maintaining therapeutic drug levels, improving bioavailability, and reducing dosing frequency which are a key objectives for oral nanomedicines [94].

Kinetic modeling of such release data often reveals an anomalous transport mechanism for chitosan-based systems, indicating that release is controlled by both diffusion and polymer relaxation/erosion [95,96]. The observed profile aligns with successful oral delivery systems for bioactive compounds, where an initial burst ensures prompt bioactivity and prolonged release enables sustained action, thereby maximizing therapeutic potential [97].

3.5. GC–MS results

GC–MS analysis was performed to confirm the successful loading of

Table 2
Cumulative percentage release of CSE from chitosan nanoparticles under simulated gastrointestinal conditions.

Time (h)	Simulated Fluid	Release (%)
0.5	SGF (pH 1.2)	19.33 ± 1.5
1.0	SGF (pH 1.2)	25.66 ± 1.2
1.5	SGF (pH 1.2)	30.50 ± 3.9
2.0	SGF → SIF Transition	32.33 ± 2.5
3.0	SIF (pH 6.8)	47.50 ± 1.8
4.0	SIF (pH 6.8)	53.67 ± 2.1
6.0	SIF (pH 6.8)	60.33 ± 1.5
8.0	SIF (pH 6.8)	67.33 ± 2.0
12.0	SIF (pH 6.8)	76.00 ± 3.4
24.0	SIF (pH 6.8)	84.00 ± 2.6

Results were expressed as mean ± SD.

Table 1
Total phenolic and flavonoid content of CSE and encapsulation parameters of CSE-CSNPs.

Sample	TPC (mg GAE/g)	TFC (mg QE/g)	EE% (TPC)	EE% (TFC)	DL% (TPC)	DL% (TFC)
Pure CSE	102.13 ± 2.93	178.90 ± 3.51	–	–	–	–
Supernatant (free extract)	27.23 ± 2.21	88.26 ± 1.11	–	–	–	–
Corn Silk Extract-Loaded CSNPs (Calculated)	74.9 ± 4.59	90.63 ± 3.11	73.2 ± 2.72	50.65 ± 0.83	16.64 ± 1.02	20.14 ± 0.69

Results were expressed as mean ± SD.

CSE phytoconstituents into CSNPs and to assess whether the nano-encapsulation process affected their chemical integrity.

The chromatographic profiles of both the pure CSE and the CSE-CSNPs showed the presence of the same twenty major bioactive compounds, confirming successful encapsulation without degradation of key constituents. The primary compounds identified were 1,2,3-propanetriol, 1-acetate, palmitic acid, and 2,3-dihydro-3,5-dihydroxy-6-methyl-4H-pyran-4-one. A slight decrease in the relative percentage of these compounds in CSE-CSNPs indicated successful integration within the polymeric matrix rather than chemical loss. The complete list of compounds with retention times and relative abundances is provided in supplementary materials (table S2).

The identified compounds are associated with a range of bioactivities that support the therapeutic potential of the formulation. 1,2,3-Propanetriol, 1-acetate is reported to possess antibacterial, anti-inflammatory, diuretic, and anticancer properties [98–100]. Palmitic acid and its derivatives (ethyl palmitate and glycerol 2-palmitate) exhibit notable antimicrobial, anti-inflammatory, and antioxidant effects, with specific roles in modulating immune responses and cholesterol levels [101–104]. The flavonoid 2,3-dihydro-3,5-dihydroxy-6-methyl-4H-pyran-4-one is a well-documented contributor to the antioxidant and anti-inflammatory activity of corn silk, attributed to its reactive enol structure [105,106]. Other significant compounds, such as ethyl linoleate and octadecanoic acid, further broaden the extract's pharmacological profile, offering reported benefits including anti-carcinogenic, cardioprotective, and antimicrobial effects [107–110].

The preservation of these bioactive compounds within the nanoparticles, as evidenced by the GC–MS profiles, confirms that the nano-encapsulation process did not compromise the phytochemical integrity of the CSE. This successful loading directly links the characterized chemical profile to the enhanced *in vitro* biological activities observed for CSE-CSNPs, providing a chemical basis for the formulation's superior performance.

3.6. *In vitro* characterization

Prior to *in vivo* application, a comprehensive *in vitro* safety and efficacy profile of CSE, blank CSNPs, and CSE-CSNPs were established. This

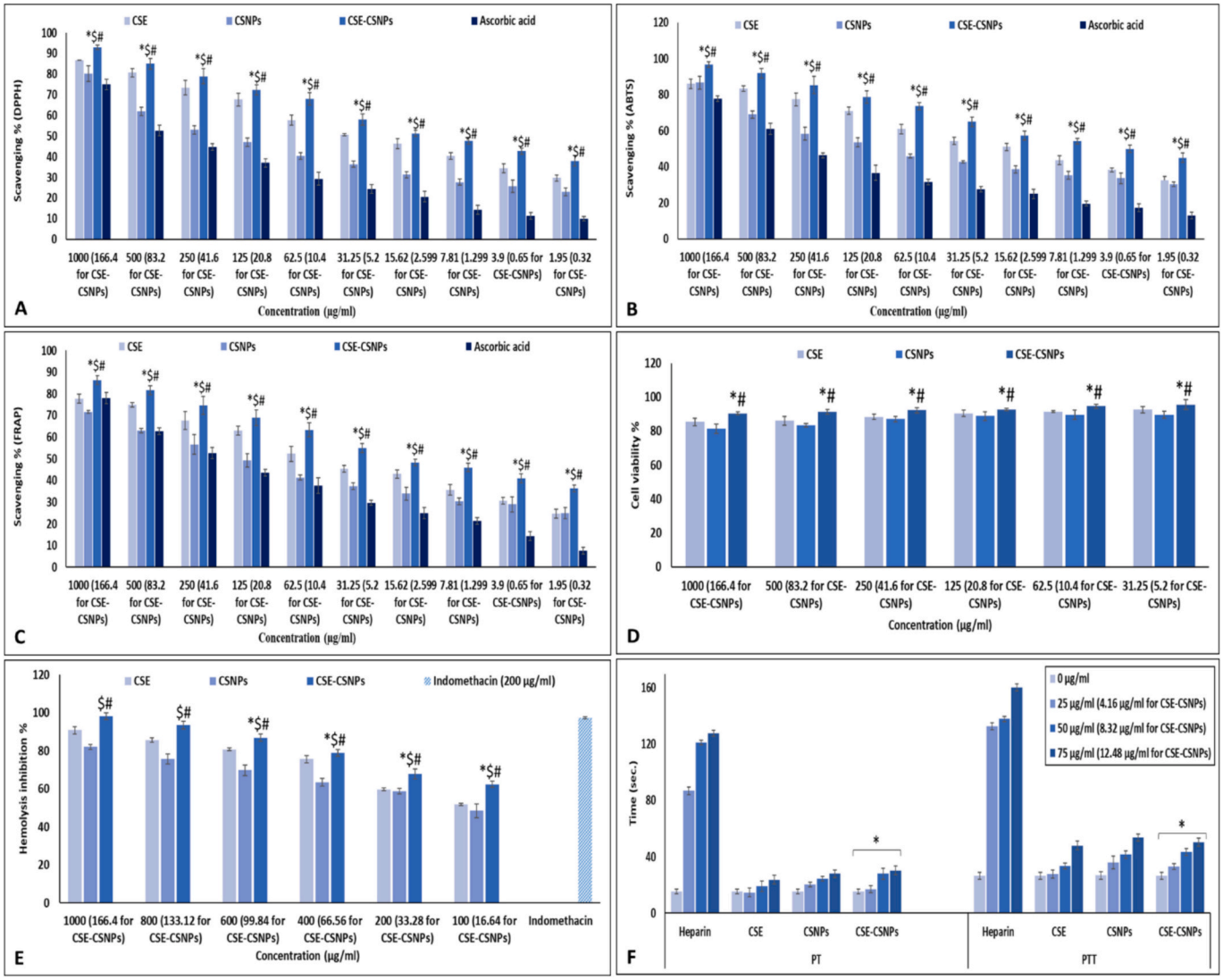

Fig. 6. *in vitro* characterization of CSE, CSNPs and CSE-CSNPs showing A] the antioxidant activity (DPPH assay) with *, $ and # represented significance ($P < 0.05$) when compared to ascorbic acid, CSE and CSNPs; B] the antioxidant activity (ABTS assay) with *, $ and # represented significance ($P < 0.05$) when compared to ascorbic acid, CSE and CSNPs; C] the antioxidant activity (FRAP test) with *, $ and # represented significance ($P < 0.05$) when compared to ascorbic acid, CSE and CSNPs; D] the cell viability % (MTT assay) with * and # represented significance ($P < 0.05$) when compared to CSE and CSNPs, respectively; E] the anti-inflammatory activity (hemolysis inhibition) with *, $ and # represented significance ($P < 0.05$) when compared to indomethacin, CSE and CSNPs, respectively; and F] the anticoagulant activity (PT and PTT) with * represented significance ($P < 0.05$) when compared to heparin.

evaluation covered antioxidant, cytotoxic, anti-inflammatory, and anticoagulant activities, providing critical insights into the biocompatibility and enhanced functionality conferred by nanoencapsulation.

Representative photographs of the actual assay outcomes for DPPH, ABTS, FRAP, hemolysis inhibition, and MTT assays are provided in Supplementary materials (fig. S1). These images visually confirm the colour changes and dose-dependent activities described below, supporting the quantitative data presented in Fig. 6.

3.6.1. Antioxidant activity (DPPH, ABTS, and FRAP assays)

The antioxidant activity of the formulations was rigorously tested *via* DPPH and ABTS radical scavenging assays and the FRAP assay (Fig. 6A–C). Quantitative analysis revealed that CSE-CSNPs achieved 93.0 ± 1.0% DPPH radical scavenging at 166.4 μg/mL, significantly higher than free CSE at 1000 μg/mL (86.7 ± 2.1%) and ascorbic acid at 1000 μg/mL (75.0 ± 2.6%). Similarly, in the ABTS assay, CSE-CSNPs at 166.4 μg/mL exhibited 96.7 ± 1.5% inhibition compared to 86.0 ± 2.6% for free CSE and 77.7 ± 1.5% for ascorbic acid. The FRAP assay confirmed these findings, with CSE-CSNPs showing 86.3 ± 2.1% reducing power at 166.4 μg/mL *versus* 77.7 ± 2.1% for free CSE and 78.0 ± 2.6% for ascorbic acid.

While free CSE showed expected dose-dependent activity, blank CSNPs exhibited minimal intrinsic antioxidant capacity. Remarkably, CSE-CSNPs displayed significantly superior antioxidant activity compared to ascorbic acid (standard), free CSE, and blank CSNPs at all equivalent concentrations. This dramatic enhancement far exceeded a simple additive effect and pointed to a synergistic phenomenon.

The enhanced antioxidant activity can be explained by several mechanisms. Nanoencapsulation in chitosan can increase the effective surface area and solubility of poorly soluble antioxidants like phenolics, shield them from premature oxidation, and improve their ability to interact with and neutralize free radicals [88,116]. The multi-mechanism confirmation across three distinct assays (DPPH, ABTS, and FRAP) strengthens the conclusion that CSE-CSNPs represent a highly potent antioxidant system.

3.6.2. Cytotoxicity (MTT assay)

The MTT assay on rat hepatocytes (Fig. 6D) provided a critical safety assessment. Quantitative analysis revealed that CSE-CSNPs maintained 90.5 ± 0.8% cell viability at 166.4 μg/mL (encapsulated extract) and 95.7 ± 3.0% at 5.2 μg/mL, values consistently higher than free CSE (85.4 ± 2.2% to 92.7 ± 1.8%) and blank CSNPs (81.5 ± 2.7% to 89.7 ± 2.2%) across all tested concentrations. CSE-CSNPs demonstrated significantly higher cell viability across all tested doses compared to both free CSE and blank CSNPs. Free CSE and blank CSNPs showed comparable viability, indicating that the chitosan carrier itself had no inherent cytotoxicity at the tested concentrations, consistent with its established biocompatibility profile [115].

The superior cytocompatibility of CSE-CSNPs suggests that nanoencapsulation may mitigate any potential cytotoxic effects of the concentrated free extract, possibly by controlling release kinetics and preventing a sudden burst of bioactive compounds that could stress cells. This finding underscores the formulation's potential for safe hepatic application.

3.6.3. Anti-inflammatory activity (Hemolysis inhibition assay)

Anti-inflammatory activity was evaluated by inhibition of hypotonicity-induced RBCs hemolysis (Fig. 6E). All samples exhibited a dose-dependent response. Free CSE showed notable activity, consistent with the known anti-inflammatory properties of plant phenolics and flavonoids [113]. Quantitative analysis revealed that CSE-CSNPs achieved 98.2 ± 1.7% hemolysis inhibition at 1000 μg/mL (166.4 μg/mL encapsulated extract), which was comparable to indomethacin (97.3 ± 0.5% at 200 μg/mL) and significantly higher than free CSE (90.8 ± 1.8% at 1000 μg/mL) and blank CSNPs (82.0 ± 1.4% at 1000 μg/mL). Even at the lowest tested concentration (16.6 μg/mL), CSE-CSNPs maintained 62.4 ± 1.6% inhibition, demonstrating dose-dependent anti-inflammatory activity.

Crucially, CSE-CSNPs exhibited significantly enhanced anti-inflammatory efficacy. At the higher tested doses (166.4 μg/mL encapsulated extract), the inhibition was statistically equivalent to the standard drug indomethacin. At lower doses (99.84 to 16.64 μg/mL), CSE-CSNPs outperformed both free CSE and blank CSNPs. This pronounced enhancement can be attributed to the nanoformulation's ability to protect encapsulated phytochemicals from degradation, improve their interaction with cellular membranes, and facilitate more efficient delivery to the site of action, as observed with other polyphenol-loaded nanocarriers [114].

3.6.4. Anticoagulant activity (PT and PTT assays)

Anticoagulant potential was assessed *via* PT and PTT (Fig. 6F). Heparin, a potent anticoagulant used as a positive control, exhibited the longest clotting times. Quantitative analysis revealed that CSE-CSNPs prolonged PT from a control value of 15.3 ± 1.5 s to 27.3 ± 3.5 s at 75 μg/mL (12.48 μg/mL encapsulated extract), and PTT from 26.3 ± 2.5 s to 50.3 ± 3.0 s, demonstrating dose-dependent anticoagulant activity. This effect was more pronounced than that of free CSE (PT: 23.7 s; PTT: 48.0 s at 75 μg/mL) and comparable to blank CSNPs (PT: 28.0 s; PTT: 53.7 s at 75 μg/mL). However, all treatments showed substantially lower anticoagulant activity than heparin (PT: 128.0 s; PTT: 160.3 s at 75 μg/mL), indicating that CSE-CSNPs exert a mild, modulatory effect without posing a significant bleeding risk.

While the clotting time for CSE-CSNPs was significantly shorter than that of heparin, it demonstrated a clear dose-dependent increase at encapsulated extract concentrations of 4.16, 8.32, and 12.48 μg/mL, suggesting a mild, modulatory anticoagulant effect. Notably, blank CSNPs also prolonged clotting time relative to the untreated control, consistent with literature reports on the inherent hemostatic-modulating properties of chitosan, a polymer known to interact with plasma proteins and platelets [111]. The activity of CSE-CSNPs likely results from a combined effect of bioactive CSE and the chitosan carrier, indicating a formulation that is hemocompatible without posing a significant bleeding risk that in turn is a crucial safety feature for a prospective therapeutic agent [112].

Collectively, these *in vitro* results demonstrate that nanoencapsulation of CSE into CSNPs transformed its biological profile. The formulation retained and amplified the desired therapeutic activities (antioxidant and anti-inflammatory) while improving biocompatibility (reduced cytotoxicity and favorable hemocompatibility). This combination, enhanced efficacy at lower bioactive doses together with improved safety, is a hallmark of successful drug delivery systems [117]. These findings strongly suggest that CSE-CSNPs can deliver the hepatoprotective phytochemicals of corn silk more efficiently and safely to target sites, providing a robust rationale for subsequent *in vivo* investigation.

3.7. In vivo experiment

The therapeutic potential of CSE-CSNPs was evaluated in a CCl_4-induced rat model of acute liver injury. The nanoformulation demonstrated superior efficacy compared to the free CSE or blank CSNPs, effectively restoring liver health across multiple pathological axes.

3.7.1. Restoration of liver function and attenuation of fibrosis

Liver function parameters: CCl_4 administration in untreated group III led to a significant increase in serum levels of liver function parameters compared to healthy control group I (Fig. 7A and B). ALT increased from 50.6 to 84.2 U/L, AST from 68.4 to 101.0 U/L, and ALP from 108.2 to 149.6 U/L. Total and direct bilirubin showed similar elevations. No significant differences were observed between control group I and vehicle group II.

Fibrosis markers: Serum fibrosis markers (laminin, hyaluronic acid,

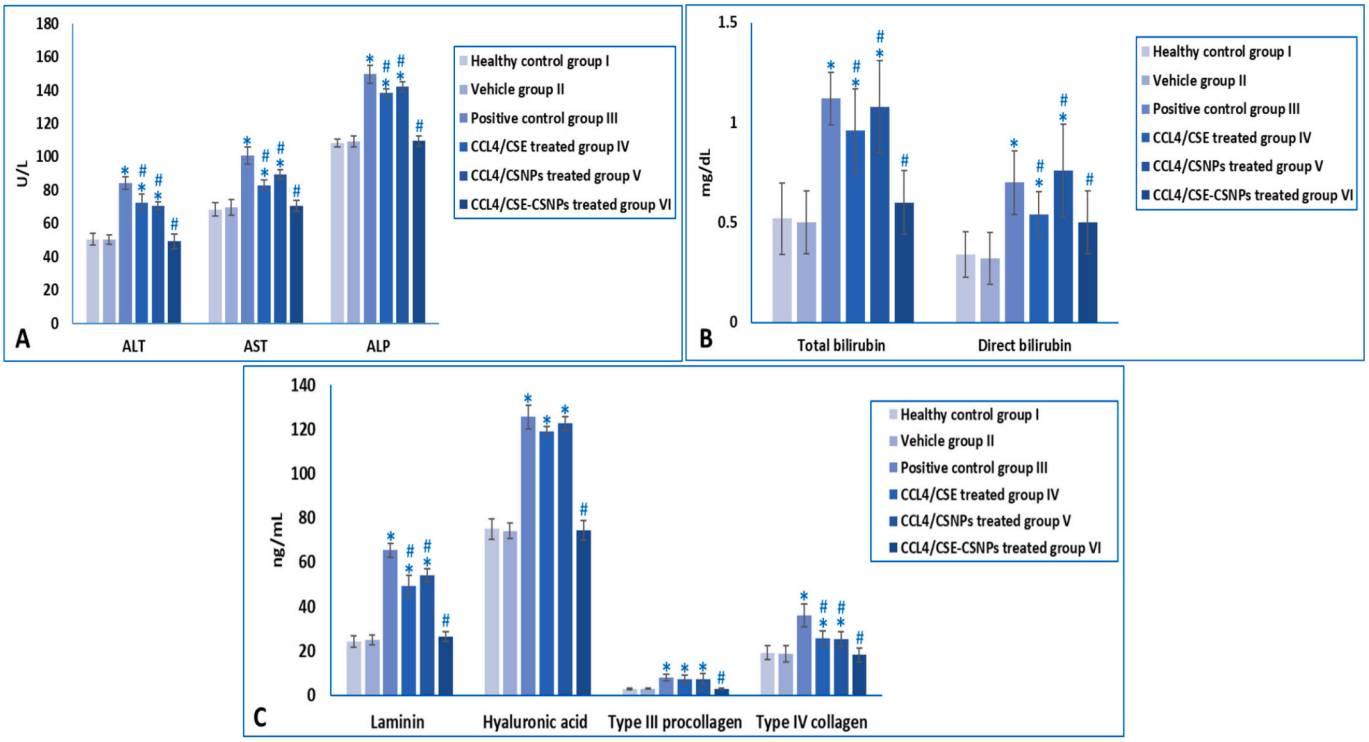

Fig. 7. Serum levels of A] ALT, AST and ALP; B] total and direct bilirubin; and C] laminin, hyaluronic acid, type III procollagen and type IV collagen in different experimental groups. * represented significance ($P < 0.05$) when compared to control group I and # represented significance ($P < 0.05$) when compared to positive control group III.

type III procollagen, and type IV collagen) were also significantly elevated in untreated group III compared to controls (Fig. 7C), confirming successful induction of liver injury and active fibrotic remodeling.

Treatment with free CSE (group IV) or blank CSNPs (group V) significantly reduced the elevated serum levels compared to positive control group III. However, these parameters remained significantly higher than those in control group I, indicating only partial recovery.

Remarkably, administration of CSE-CSNPs (group VI) completely ameliorated CCl_4-induced liver damage. No significant differences were observed between treated group VI and healthy control group I for any of the measured parameters (ALT, AST, ALP, bilirubin, laminin, hyaluronic acid, type III procollagen, or type IV collagen).

This complete restoration highlights a synergistic effect whereby the chitosan nanoparticle carrier potentiates the intrinsic hepatoprotective properties of corn silk. Corn silk is historically recognized for its medicinal properties, including anti-inflammatory and antioxidant activities [118–124]. Nanoencapsulation overcomes key limitations of traditional herbal extracts, such as poor bioavailability, pH sensitivity, and enzymatic degradation in the gastrointestinal tract [125–127]. The enhanced efficacy at a lower bioactive dose—100 mg/kg CSE-CSNPs delivering approximately 16.6 mg/kg of encapsulated CSE compared to 200 mg/kg free CSE—directly demonstrates the success of the delivery system in enhancing bioavailability and target engagement.

3.7.2. *Amelioration of oxidative stress and inflammation*

Oxidative stress markers: CCl_4 toxicity is mediated by the generation of free radicals, leading to lipid peroxidation and depletion of endogenous antioxidants. This was confirmed in untreated group III by a marked increase in hepatic MDA (11.0 *vs.* 24.0 ng/mg protein) and decreases in GSH (97.2 *vs.* 55.4 μg/mg protein), CAT (63.4 *vs.* 22.2 U/mg protein), and SOD (54.4 *vs.* 31.2 U/mg protein) compared to healthy controls (Fig. 8A-D).

While free CSE and blank CSNPs showed significant antioxidant activity, only CSE-CSNPs fully restored all oxidative stress parameters to baseline control levels (MDA: 10.6 ng/mg protein, GSH: 97.6 μg/mg protein, CAT: 63.4 U/mg protein, SOD: 55.2 U/mg protein). The superior antioxidant performance of the nanoformulation can be attributed to its ability to protect bioactive compounds, ensure sustained release, and improve cellular uptake [128,129].

Inflammatory markers: The inflammatory cascade triggered by CCl_4 was confirmed by marked elevations in pro-inflammatory cytokines in untreated group III compared to healthy controls: IL-1β increased from 82.8 to 261 pg/g tissue, IL-17 from 70.8 to 199.8 pg/g tissue, TNF-α from 213 to 487.6 pg/g tissue, and IL-18 from 103.4 to 256.2 pg/g tissue (Fig. 9). Additionally, the anti-inflammatory cytokine IL-10 increased from 100.6 to 394.4 pg/g tissue, indicating a compensatory anti-inflammatory response.

Treatment with free CSE or blank CSNPs significantly reduced these cytokine levels, but they remained elevated compared to controls. In contrast, CSE-CSNPs completely normalized all cytokine levels to values comparable with healthy controls (IL-1β: 82.6, IL-17: 78.6, TNF-α: 218.6, IL-18: 108.2, IL-10: 106.6 pg/g tissue).

This potent anti-inflammatory effect aligns with the documented activity of corn silk phytochemicals [121,122] and is significantly amplified by nano-delivery, which enhances residence time and interaction with immune cells.

3.7.3. *Apoptosis evaluation in liver tissue homogenates*

Apoptosis was evaluated by measuring the pro-apoptotic proteins (Bax, p53, caspase 3, and caspase 8) and the anti-apoptotic protein Bcl2 in liver tissue homogenates using ELISA kits.

CCl_4 administration led to induced apoptosis in liver. Untreated group III showed a significant elevation in pro-apoptotic proteins and a significant reduction in Bcl2 compared to healthy control group I. Specifically, Bax increased from 353.2 to 575.6 pg/g tissue, p53 from 1.06 to 4.00 ng/g tissue, caspase 3 from 20.6 to 67.0 pmol/g tissue, and caspase 8 from 0.38 to 2.74 ng/g tissue, while Bcl2 decreased from 5.88

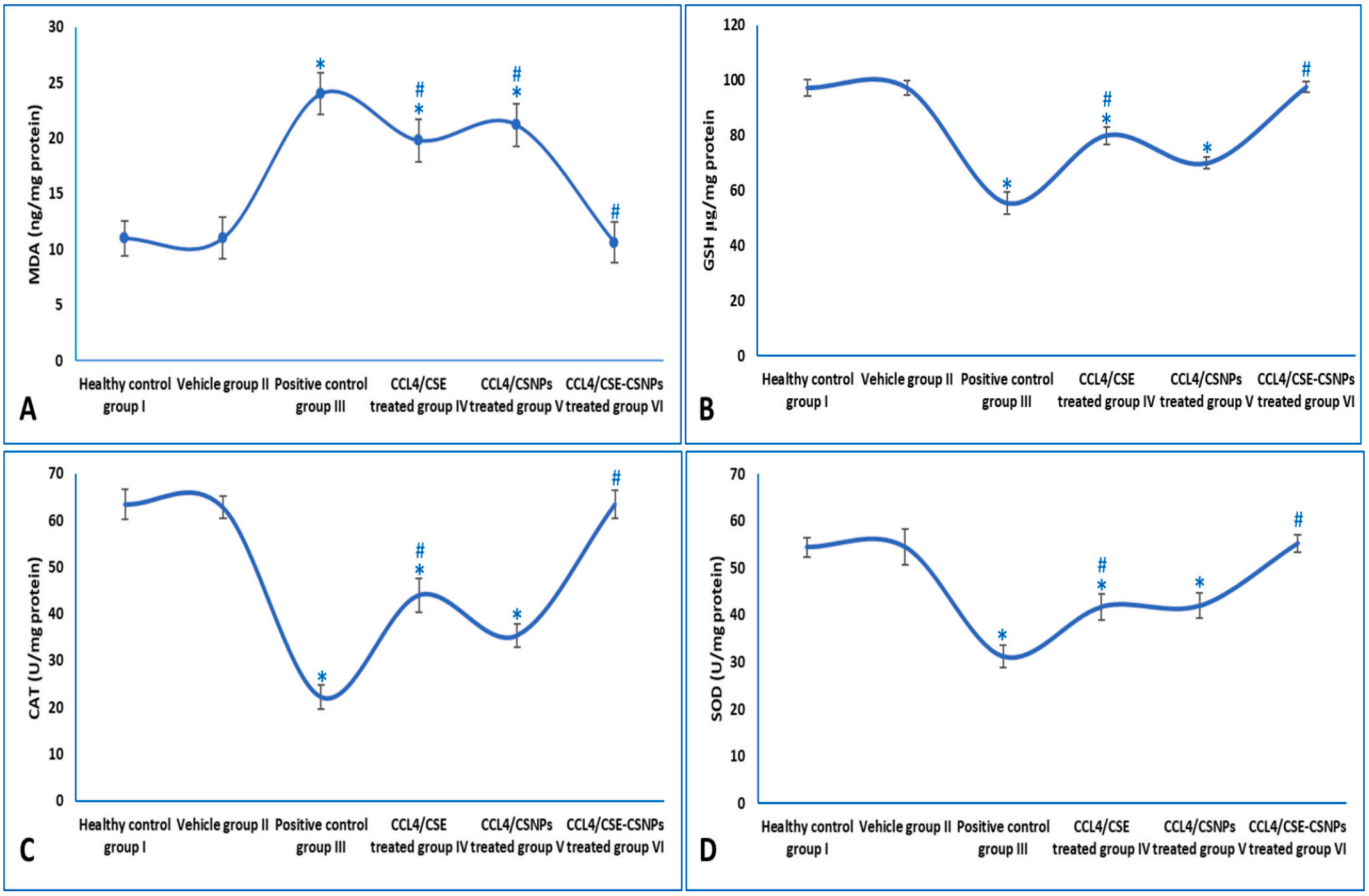

Fig. 8. Oxidative stress evaluation showing levels of A] MDA, B] GSH, C] CAT and D] SOD in liver tissue homogenates of different experimental groups. * represented significance ($P < 0.05$) when compared to control group I and # represented significance ($P < 0.05$) when compared to positive control group III.

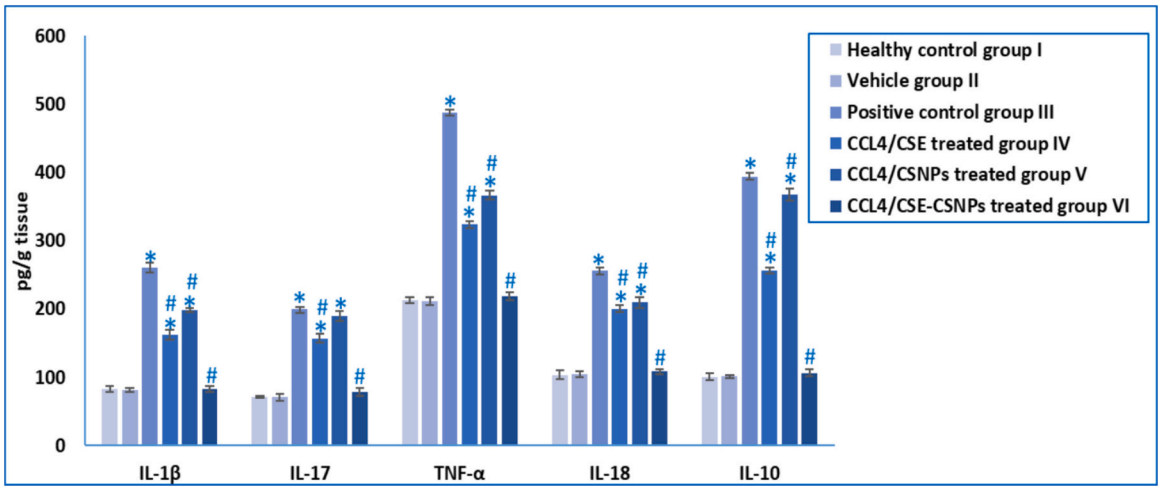

Fig. 9. Cytokines (IL-1β, IL-17, TNF-α, IL-18 and IL-10) levels in liver tissue homogenates of different experimental groups. * represented significance ($P < 0.05$) when compared to control group I and # represented significance ($P < 0.05$) when compared to positive control group III.

to 3.96 ng/g tissue (Fig. 10A-D). No significant differences were observed between control group I and vehicle group II.

Treatment with free CSE (group IV) or blank CSNPs (group V) significantly elevated Bcl2 levels and reduced pro-apoptotic protein levels compared to positive control group III. However, these parameters remained significantly different from control values, indicating only partial protection. Remarkably, no significant differences were observed in any apoptotic marker when comparing CSE-CSNPs-treated group VI with healthy control group I. CSE-CSNPs restored Bcl2 to 5.68 ng/g tissue, Bax to 353.4 pg/g tissue, p53 to 1.10 ng/g tissue, caspase 3 to 20.0 pmol/g tissue, and caspase 8 to 0.56 ng/g tissue (all comparable to control values). This robust cytoprotection suggests that the nanoformulation not only neutralizes toxic insults but also actively supports cell survival pathways, further demonstrating the superior therapeutic efficacy of CSE-CSNPs over free CSE or blank CSNPs.

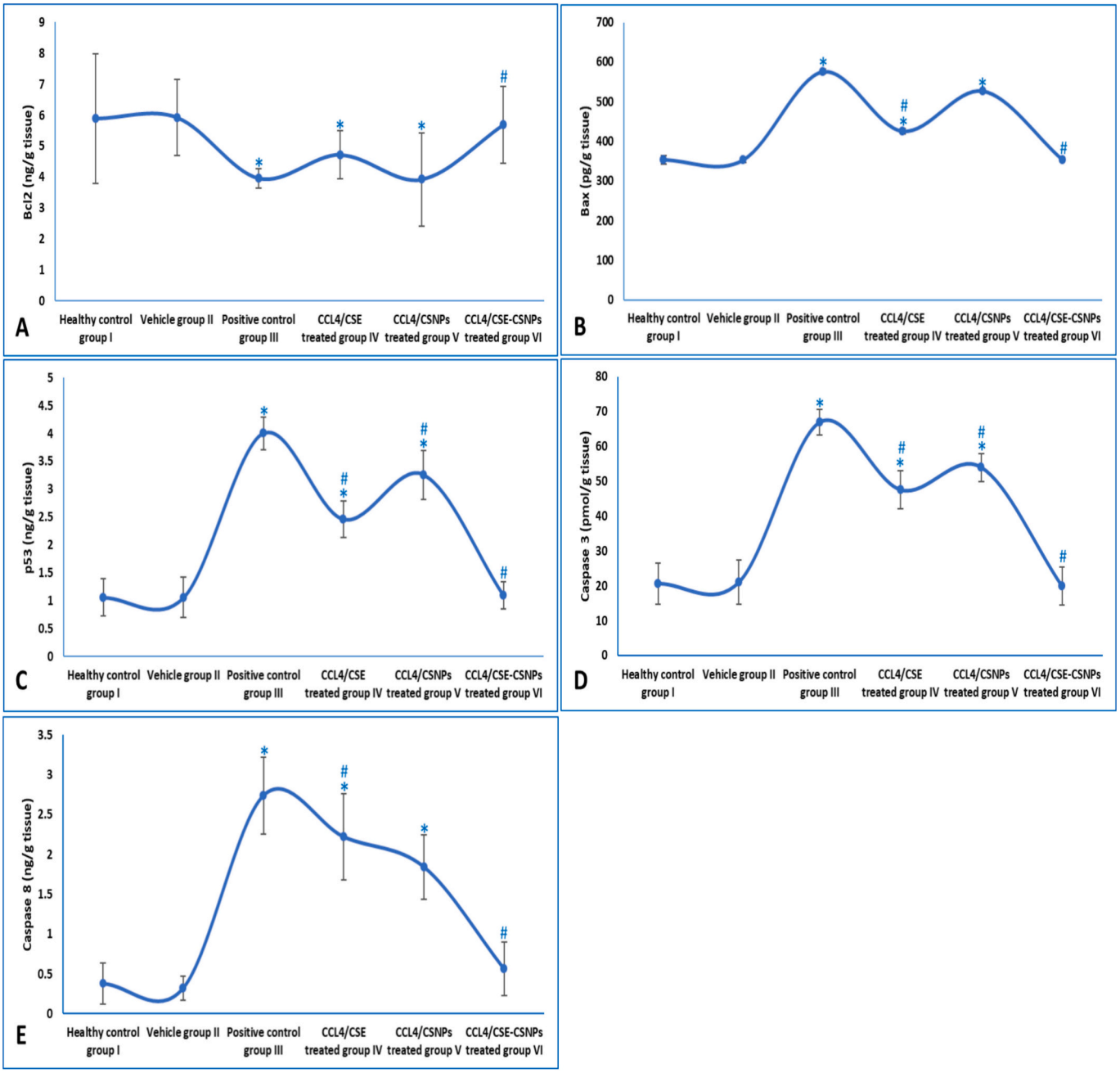

Fig. 10. Apoptotic markers evaluation showing levels of A] Bcl2, B] Bax, C] p53, D] caspase 3 and E] caspase 8 in liver tissue homogenates of different experimental groups. * represented significance ($P < 0.05$) when compared to control group I and # represented significance ($P < 0.05$) when compared to positive control group III.

3.7.4. Liver remodeling evaluation in liver tissue homogenates

Liver remodeling was evaluated by measuring MMP9 and TIMP1 in liver tissue homogenates. Untreated group III showed significantly elevated levels of both markers compared to healthy control group I, indicating active tissue remodeling and fibrosis progression. MMP9 increased from 5.94 to 16.26 ng/g tissue, and TIMP1 increased from 149.2 to 313.0 pg/g tissue (Fig. 11A-B). No significant differences were observed between control group I and vehicle group II.

Treatment with free CSE (group IV) or blank CSNPs (group V) reduced MMP9 and TIMP1 levels compared to untreated group III. However, both markers remained elevated compared to controls, with CSE showing greater reduction than CSNPs. Notably, no significant differences were observed in MMP9 or TIMP1 levels between CSE-CSNPs-treated group VI and healthy control group I. CSE-CSNPs restored MMP9 to 6.12 ng/g tissue and TIMP1 to 148.0 pg/g tissue, values comparable to controls, indicating normalized tissue repair dynamics and prevention of aberrant fibrosis.

The collective *in vivo* data presents a compelling case for CSE-CSNPs as a superior therapeutic agent. The free CSE possesses inherent bioactivity, but its effects are partial and require a higher dose. The blank CSNPs show modest protective effects, likely due to chitosan's own documented antioxidant and anti-inflammatory properties [130,131]. However, the CSE-CSNP formulation achieved complete hepatoprotection across all measured parameters (liver function, oxidative stress, inflammation, apoptosis, and fibrosis). This dramatic improvement can be attributed to the fundamental advantages of the nano-drug delivery system. CSNPs, formed *via* ionic gelation, efficiently encapsulate hydrophobic plant extracts through matrix entrapment and surface

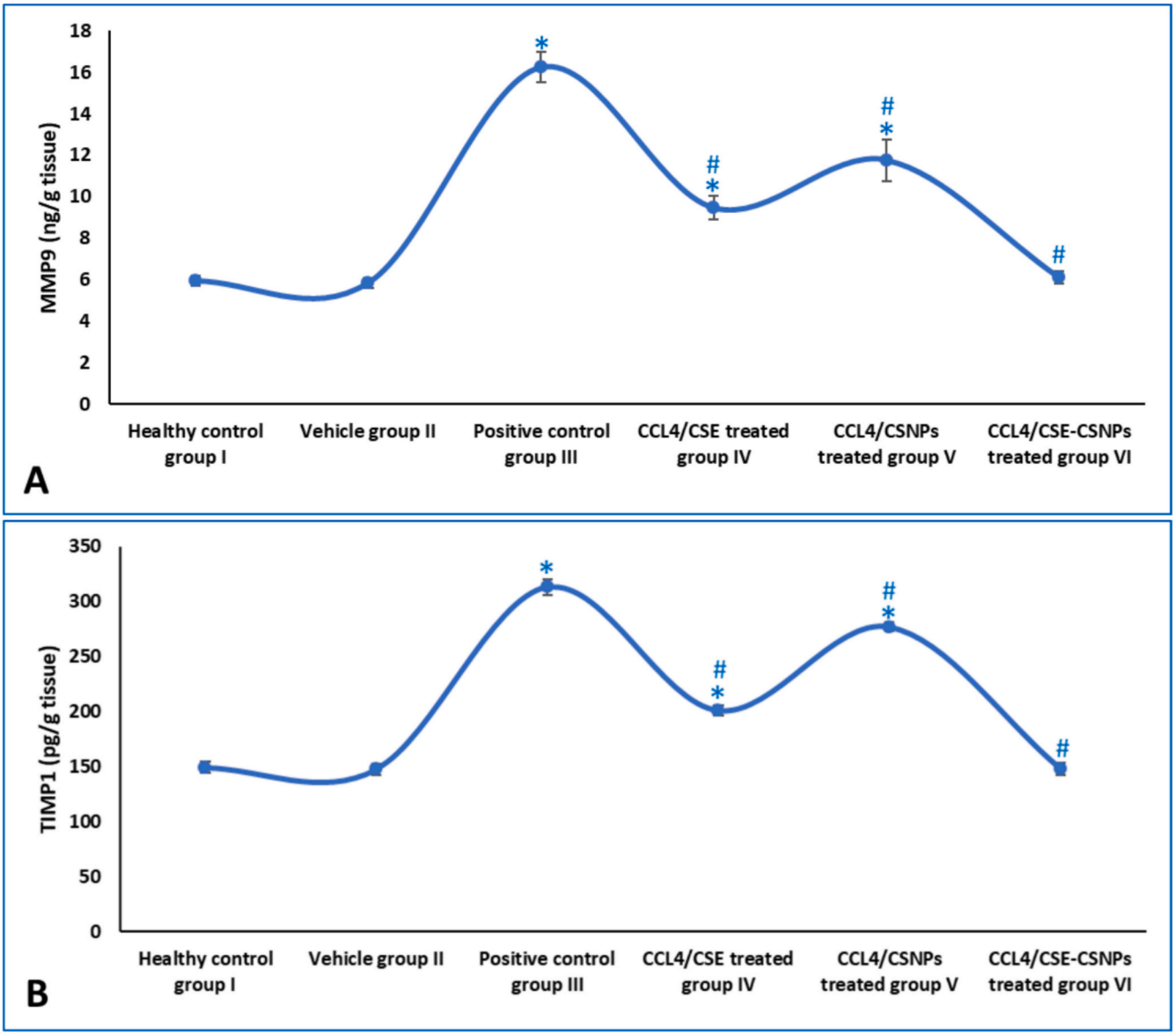

Fig. 11. Levels of A] MMP9 and B] TIMP1 in liver tissue homogenates of different experimental groups. * represented significance ($P < 0.05$) when compared to control group I and # represented significance ($P < 0.05$) when compared to positive control group III.

adsorption [79,132]. Their small size, positive charge, and mucoadhesive properties promote GI absorption and liver targeting [80,81]. Crucially, the biphasic release profile—initial burst followed by sustained release—ensures both immediate therapeutic intervention and prolonged action, maximizing the multi-target effects of the CSE phytochemicals. This study exemplifies how nanotechnology can transform a traditional medicinal extract into a potent, targeted, and comprehensive therapeutic formulation, validating its potential for treating liver diseases.

4. Conclusion

This study successfully developed and characterized CSE-CSNPs using the ionic gelation method, representing the first investigation of this nanoformulation for hepatoprotection. The nanoparticles exhibited favorable physicochemical properties, including small size (49.61–51.12 nm), high positive surface charge (+45.61 mV), and efficient encapsulation of phenolic and flavonoid compounds, with a biphasic release profile suitable for oral delivery.

Comprehensive *in vitro* evaluation confirmed the biocompatibility, enhanced antioxidant activity, and superior anti-inflammatory effects of CSE-CSNPs compared to free extract. In a CCl_4-induced acute liver injury rat model, the nanoformulation demonstrated remarkable therapeutic efficacy, completely restoring liver function parameters (ALT, AST, ALP, bilirubin), oxidative stress markers (MDA, GSH, SOD, CAT), and pro-inflammatory cytokine levels (IL-1β, TNF-α) to healthy control values—achieving full hepatoprotection at half the dose of free CSE. Additionally, CSE-CSNPs effectively normalized apoptotic pathways (Bax, Bcl2, caspase 3, caspase 8) and tissue remodeling markers (MMP9, TIMP1), indicating comprehensive mitigation of the multifaceted pathology of drug-induced liver injury.

The enhanced therapeutic efficacy of CSE-CSNPs is attributed to the synergistic combination of corn silk's intrinsic bioactive properties with the advanced delivery capabilities of CSNPs, including protection from gastrointestinal degradation, enhanced mucoadhesion, sustained release, and improved cellular uptake. These findings establish proof-of-concept that chitosan nanoencapsulation significantly enhances the bioavailability and therapeutic potency of corn silk bioactives.

While the study provides strong preliminary evidence for the efficacy of CSE-CSNPs, we acknowledge some limitations: 1- the use of a single

dose in an acute injury model and the sample size, while adequate for demonstrating significant effects, represent a focused scope. Future work should explore dose-response relationships, evaluate efficacy in other chronic liver disease models, and assess long-term safety profiles. Collectively, this study positions CSE-CSNPs as a promising nano-therapeutic strategy that bridges traditional herbal medicine with modern drug delivery technology, offering a potential alternative for the management of DILI.

CRediT authorship contribution statement

Alyaa Farid: Writing – review & editing, Writing – original draft, Methodology, Conceptualization. **Aya Badawi:** Writing – original draft, Methodology, Conceptualization. **Malak Waheed:** Writing – original draft, Methodology, Conceptualization. **Mohamed Ashraf:** Writing – original draft, Methodology, Conceptualization. **Maryam Amr:** Writing – review & editing, Writing – original draft, Methodology, Conceptualization. **Ayman Amin:** Writing – original draft, Conceptualization.

Consent for publication

Not applicable.

Ethics approval and consent to participate

All experimental procedures were carried out in accordance with the international guidelines for the care and use of laboratory animals, and the study was conducted in accordance with the guide for the care and use of laboratory animals, Eighth edition (2011). All experiment procedures were approved by the Institutional Animal Care and Use Committee of October University for Modern Sciences and Arts.

Funding

This research did not receive any specific grant from funding agencies in the public, commercial, or not-for-profit sectors.

Declaration of competing interest

The authors declare that they have no known competing financial interests or personal relationships that could have appeared to influence the work reported in this paper.

Appendix A. Supplementary data

Supplementary data to this article can be found online at https://doi.org/10.1016/j.ijbiomac.2026.152961.

Data availability

Data will be made available on request.

References

[1] D.A. Smith, E.F. Schmid, Drug withdrawals and the lessons within, Curr. Opin. Drug Discov. Devel. 9 (1) (2006) 38–46.
[2] G. Ostapowicz, R.J. Fontana, F.V. Schiødt, A. Larson, T.J. Davern, S.H. Han, T. M. McCashland, A.O. Shakil, J.E. Hay, L. Hynan, J.S. Crippin, A.T. Blei, G. Samuel, J. Reisch, W.M. Lee, U.S. Acute liver failure study group, Results of a prospective study of acute liver failure at 17 tertiary care centers in the United States, Ann. Intern. Med. 137 (12) (2002) 947–954.
[3] C. Lammert, E. Bjornsson, A. Niklasson, N. Chalasani, Oral medications with significant hepatic metabolism at higher risk for hepatic adverse events, Hepatology 51 (2) (2010) 615–620.
[4] V.R. Ballotin, L.G. Bigarella, A.B.M. Brandão, R.A. Balbinot, S.S. Balbinot, J. Soldera, Herb-induced liver injury: systematic review and meta-analysis, World J. Clin. Cases 9 (20) (2021) 5490–5513.
[5] D.J. Antoine, D.P. Williams, B.K. Park, Understanding the role of reactive metabolites in drug-induced hepatotoxicity: state of the science, Expert Opin. Drug Metab. Toxicol. 4 (11) (2008) 1415–1427.
[6] B.K. Park, N.R. Kitteringham, J.L. Maggs, M. Pirmohamed, D.P. Williams, The role of metabolic activation in drug-induced hepatotoxicity, Annu. Rev. Pharmacol. Toxicol. 45 (2005) 177–202.
[7] A. Berson, S. Renault, P. Lettéron, M.A. Robin, B. Fromenty, D. Fau, M.A. Le Bo, C. Riché, A.M. Durand-Schneider, G. Feldmann, D. Pessayre, Uncoupling of rat and human mitochondria: a possible explanation for tacrine-induced liver dysfunction, Gastroenterology 110 (6) (1996) 1878–1890.
[8] M. Leist, B. Single, A.F. Castoldi, S. Kühnle, P. Nicotera, Intracellular adenosine triphosphate (ATP) concentration: a switch in the decision between apoptosis and necrosis, J. Exp. Med. 185 (8) (1997) 1481–1486.
[9] D.B. Njoku, R.S. Greenberg, M. Bourdi, C.B. Borkowf, E.M. Dake, J.L. Martin, L. R. Pohl, Autoantibodies associated with volatile anesthetic hepatitis found in the sera of a large cohort of pediatric anesthesiologists, Anesth. Analg. 94 (2) (2002) 243–249.
[10] M.P. Holt, C. Ju, Mechanisms of drug-induced liver injury, AAPS J. 8 (1) (2006) E48–E54.
[11] J.W. Clinton, S. Kiparizoska, S. Aggarwal, S. Woo, W. Davis, J.H. Lewis, Drug-induced liver injury: highlights and controversies in the recent literature, Drug Saf. 44 (2021) 1125–1149.
[12] A.L. Gerbes, Drug-induced liver injury (DILI): a major challenge, Drug Res. 71 (2021) S7.
[13] A. Rodríguez, I. García-García, L. Soto, A. Huertas, A. Borobia, A. González-Torbay, I. Akatbach-Bousaid, M. González-Muñoz, E. Ramirez, Utility of lymphoycyte transformation test for assisting updated Roussel Uclaf causality assessment method in drug-induced liver injury: a case-control study, Front. Pharmacol. 13 (2022) 819589.
[14] R.A. Wurzburger, Case of delayed hepatic injury associated with teriflunomide use as assessed for causality using the updated RUCAM, Case Rep. Hepatol. 2022 (2022) 6331923.
[15] M.S. Benić, L. Nežić, V. Vujić-Aleksić, L. Mititelu-Tartau, Novel therapies for the treatment of drug-induced liver injury: a systematic review, Front. Pharmacol. 12 (2022) 785790.
[16] Y.K. Gupta, M. Sharma, G. Chaudhary, Pyrogallol-induced hepatotoxicity in rats: a model to evaluate antioxidant hepatoprotective agents, Methods Find. Exp. Clin. Pharmacol. 24 (2002) 497–500.
[17] Y.K. Gupta, M. Sharma, G. Chaudhary, C.K. Katiyar, Hepatoprotective effect of new Livfit, a polyherbal formulation, is mediated through its free radical scavenging activity, Phytother. Res. 18 (2004) 362–364.
[18] G. Upadhyay, A. Kumar, M.P. Singh, Effect of silymarin on pyrogallol- and rifampicin-induced hepatotoxicity in mouse, Eur. J. Pharmacol. 565 (2007) 190–201.
[19] Z.A. Maksimovic, N. Kovacevic, Preliminary assay on the antioxidative activity of Maydis stigma extracts, Fitoterapia 74 (2003) 144–147.
[20] B.B. Wei, Z.X. Chen, M.Y. Liu, M.J. Wei, Development of a UPLC-MS/MS method for simultaneous determination of six flavonoids in rat plasma after administration of maydis stigma extract and its application to a comparative pharmacokinetic study in normal and diabetic rats, Molecules 22 (8) (2017) 1267.
[21] N. Aukkanit, T. Kemngoen, N. Ponharn, Utilization of corn silk in low fat meatballs and its characteristics, Procedia. Soc. Behav. Sci. 197 (2014) 1403–1410.
[22] S.H. Ren, Q.Q. Qiao, X.L. Ding, Antioxidant activity of five flavones glycosides from corn silk (stigma maydis), Czech J. Food Sci. 2 (2013) 148–155.
[23] Q.L. Hu, Z. Deng, Protective effects of flavonoids from corn silk on oxidative stress induced by exhaustive exercise in mice, Afr. J. Biotechnol. 10 (2011) 3163–3167.
[24] K. Bhuvaneshwari, S. Sridevi, Analysis of nutrients and photochemical contents in corn silk (Zea Mays), Int. J. Sci. Res. 78 (2015) 2319–7064.
[25] S. Zilic, M. Jankovic, Z. Basic, J. Vancetovic, V. Maksimovic, Antioxidant activity, phenolic profile, chlorophyll and mineral matter content of corn silk (Zea mays L.): comparison with medicinal herbs, J. Cereal Sci. 69 (2016) 363–370.
[26] F. Amreen, P. Agrawal, P.P. Singh, Herbal option for diabetes: an overview, Asian Pac. J. Trop. Dis. 2 (2012) S536–S544.
[27] W. Zhao, Y. Yin, Z. Yu, J. Liu, F. Chen, Comparison of anti-diabetic effects of polysaccharides from corn silk on normal and hyperglycemia rats, Int. J. Biol. Macromol. 50 (2012) 1133–1137.
[28] S. Chen, H. Chen, J. Tian, Y. Wang, L. Xing, J. Wang, Chemical modification, antioxidant and α-amylase inhibitory activities of corn silk polysaccharides, Carbohydr. Polym. 2 (2013) 536–544.
[29] J. Singh, B.S. Inbaraj, S. Kaur, P. Rasane, V. Nanda, Phytochemical analysis and characterization of corn silk (*Zea mays*, G5417), Agronomy 12 (4) (2022) 777.
[30] C. Wang, T. Zhang, S. Liu, C. Zhang, E. Wang, Z. Wang, Y. Zhang, J. Liu, Subchronic toxicity study of corn silk with rats, J. Ethnopharmacol. 137 (2011) 36–43.
[31] S. Saheed, A.E. Oladipipo, A.A. Abdulazeez, S.A. Olarewaju, N.O. Ismaila, I. A. Emmanuel, Q.D. Fatimah, A.Y. Aisha, Toxicological evaluations of stigma maydis (corn silk) aqueous extract on hematological and lipid parameters in Wistar rats, Toxicol. Rep. 2 (2012) 638–644.
[32] M.J. Lis, Ó.G. Carmona, C.G. Carmona, F.M. Bezerra, Inclusion complexes of citronella oil with β-cyclodextrin for controlled release in biofunctional textiles, Polymers 10 (2018) 1324.
[33] E. Mele, Electrospinning of essential oils, Polymers 12 (2020) 908.

[34] B. Mishra, B.B. Patel, S. Tiwari, Colloidal nanocarriers: a review on formulation technology, types and applications toward targeted drug delivery, Nanomedicine (Philadelphia, Pa.) 6 (2010) 9–24.
[35] B.R. Rizeq, N.N. Younes, K. Rasool, G.K. Nasrallah, Synthesis, bioapplications, and toxicity evaluation of chitosan-based nanoparticles, Int. J. Mol. Sci. 20 (2019) 5776.
[36] C.A. Campos, L.N. Gerschenson, S.K. Flores, Development of edible films and coatings with antimicrobial activity, Food Bioprocess Technol. 4 (2010) 849–875.
[37] R.A.I. Reshad, T.A. Jishan, N.N. Chowdhury, Chitosan and its broad applications: a brief review, J. Clin. Exp. Investig. 12 (2021) em00779.
[38] E.I. Rabea, M.E.T. Badawy, C.V. Stevens, G. Smagghe, W. Steurbaut, Chitosan as antimicrobial agent: applications and mode of action, Biomacromolecules 4 (2003) 1457–1465.
[39] M. Kong, X.G. Chen, K. Xing, H.J. Park, Antimicrobial properties of chitosan and mode of action: a state of the art review, Int. J. Food Microbiol. 144 (2010) 51–63.
[40] D. Zhao, S. Yu, B. Sun, S. Gao, S. Guo, K. Zhao, Biomedical applications of chitosan and its derivative nanoparticles, Polymers 10 (2018) 462.
[41] N. Morin-Crini, E. Lichtfouse, G. Torri, G. Crini, Applications of chitosan in food, pharmaceuticals, medicine, cosmetics, agriculture, textiles, pulp and paper, biotechnology, and environmental chemistry, Environ. Chem. Lett. 17 (2019) 1667–1692.
[42] X. Xiong Chang, N. Mujawar Mubarak, S. Ali Mazari, A. Sattar Jatoi, A. Ahmad, M. Khalid, R. Walvekar, E.C. Abdullah, R.R. Karri, M.T. Siddiqui, A review on the properties and applications of chitosan, cellulose and deep eutectic solvent in green chemistry, J. Ind. Eng. Chem. 104 (2021) 362–380.
[43] N. Thaiwong, Drying temperature of corn silk tea: physical properties, total phenolic content, antioxidant activity and flavonoid content, Food Appl Biosci J 8 (3) (2020) 38–48.
[44] L. Zhang, Y. Yang, Z. Wang, Extraction optimization of polysaccharides from corn silk and their antioxidant activities in vitro and in vivo, Front. Pharmacol. 4 (2021) 2328.
[45] AOAC, Official methods of analysis, 18th ed., Association of Official Analytical Chemists, Arlington, VA, USA, 2005.
[46] Y.M. Ho, W.A. Nizam, W.R. Rosli, Y.M. Ho, W.A. Wan Amir Nizam, W. Wan Rosli, Antioxidative activities and polyphenolic content of different varieties of Malaysian young corn ear and cornsilk, Sains Malaysiana 45 (2016) 195–200.
[47] S. Ranganna, Handbook of Analysis and Quality Control for Fruit and Vegetable Products, Tata Mcgraw Hill, New Delhi, India, 2006.
[48] V. Prakash, S. Saxena, S. Gupta, A.K. Saxena, R. Yadav, S.K. Singh, Preliminary phytochemical screening and biological activities of Adina cardifolia, J Microb Biochem Technol 7 (2015) 33–38.
[49] J.M. Dahanayake, P.K. Perera, P.G. Galappatty, P. Fernando, M. Arawwawala, Pharmacognostical, physico-chemical and phytochemical evaluation for standardization of three *Piper species* used in Ayurvedic medicine, Asian J. Pharmacogn. 3 (2) (2019) 18–28.
[50] C. Limmatvapirat, C. Nateesathittarn, K. Dechasathian, T. Moohummad, P. Chinajitphan, S. Limmatvapirat, Phytochemical analysis of baby corn silk extracts, Journal of Ayurveda and Integrative Medicine 11 (3) (2020) 344–351.
[51] P. Harika, B. Kannamba, G.V. Ramana, B. Haribabu, Effect of solvent composition on total phenol and §avonoids content of *Withania somnifera*, J. Chem. Pharm. Sci. 10 (2017) 601–603.
[52] B.P. Ezhilan, R. Neelamegam, GC-MS analysis of phytocomponents in the ethanol extract of Polygonum chinense L, Pharm. Res. 4 (1) (2012) 11.
[53] E. Sarepoua, R. Tangwongchai, B. Suriharn, K. Lertrat, Relationships between phytochemicals and antioxidant activity in corn silk, Int. Food Res. J. 20 (5) (2013) 2073.
[54] R. Zhang, L. Huang, Y. Deng, J. Chi, Y. Zhang, Z. Wei, M. Zhang, Phenolic content and antioxidant activity of eight representative sweet corn varieties grown in South China, Int. J. Food Prop. 20 (12) (2017) 3043–3055.
[55] M. Negm, N. Ahmed, L. Barakat, The role of curcumin – chitosan nanoparticles in the prevention and treatment of liver fibrosis in mice, Alfarama Journal of Basic & Applied Sciences 3 (2022) 8–28.
[56] M. Alfawaz, E.M. Elmorsy, A.N. Alshammari, N.A. Hakim, N.M.M. Jawad, S. A. Hassan, M.S. Fawzy, S.E. Esmaeel, Carvacrol-loaded chitosan nanoparticles as a multifunctional nanotherapeutic strategy targeting oxidative stress, inflammation, apoptosis, and genotoxicity in nonalcoholic fatty liver disease, Antioxidants 14 (2025) 1432.
[57] O. Ashraf, A. Farid, G. Safwat, Preparation of Aloe vera extract-loaded chitosan nanoparticles for the controlled delivery of extract phytochemicals in carbon tetrachloride-induced liver injury rat model, Beni-Suef Univ J Basic Appl Sci 14 (2025) 74.
[58] O.T. Somade, B.O. Ajayi, O.E. Olunaike, L.A. Jimoh, Hepatic oxidative stress, up-regulation of pro-inflammatory cytokines, apoptotic and oncogenic markers following 2-methoxyethanol administrations in rats, Biochem. Biophys. Rep. 24 (2020) 100806.
[59] J.M. Antoine, L.A.H. Fung, C.N. Grant, H.T. Dennis, G.C. Lalor, Dietary intake of minerals and trace elements in rice on the Jamaican market, J. Food Compos. Anal. 26 (2012) 111–121.
[60] A.R. Nurhanan, W.I.W. Rosli, Nutritional compositions and antioxidative capacity of the silk obtained from immature and mature corn, J. King Saud Univ. - Sci. 26 (2014) 119–127.
[61] W.I.W. Rosli, N.S. Suhaiminudin, Mineral composition, heavy metal and sensory acceptability of drink developed from corn silk (Zea mays hairs), Adv. Nat. Appl. Sci. 14 (2020) 14–19.
[62] D. Lin, M. Xiao, J. Zhao, Z. Li, B. Xing, X. Li, M. Kong, L. Li, Q. Zhang, Y. Liu, H. Chen, An overview of plant phenolic compounds and their importance in human nutrition and management of type 2 diabetes, Molecules 21 (10) (2016) 1374.
[63] M. Heinrich, J. Mah, V. Amirkia, Alkaloids used as medicines: structural phytochemistry meets biodiversity —an update and forward look, Molecules 26 (7) (2021) 1836.
[64] A.P. Ambrosy, J. Butler, A. Ahmed, M. Vaduganathan, D.J. Van Veldhuisen, W. S. Colucci, M. Gheorghiade, The use of digoxin in patients with worsening chronic heart failure: reconsidering an old drug to reduce hospital admissions, J. Am. Coll. Cardiol. 63 (18) (2014) 1823–1832.
[65] A. Grenha, Chitosan nanoparticles: a survey of preparation methods, J. Drug Target. 20 (2012) 291–300.
[66] S. Naskar, S. Sharma, K. Kuotsu, Chitosan-based nanoparticles: an overview of biomedical applications and its preparation, J. Drug Delivery Sci. Technol. 49 (2019) 66–81.
[67] T.D. Tavares, J.C. Antunes, F. Ferreira, H.P. Felgueiras, Biofunctionalization of natural fiber-reinforced biocomposites for biomedical applications, Biomolecules 10 (2020) 148.
[68] J.C. Antunes, C.L. Pereira, M. Molinos, F. Ferreira-Da-Silva, M. Dessi, A. Gloria, L. Ambrosio, R.M. Gonçalves, M.A. Barbosa, Layer-by-layer self-assembly of chitosan and poly(γ-glutamic acid) into polyelectrolyte complexes, Biomacromolecules 12 (2011) 4183–4195.
[69] J. Antunes, R. Gonçalves, M. Barbosa, Chitosan/poly(γ-glutamic acid) polyelectrolyte complexes: from self-assembly to application in biomolecules delivery and regenerative medicine, Res. Rev. J. Mater. Sci. 4 (4) (2016) 12–36.
[70] N. Babayevska, Ł. Przysiecka, I. Iatsunskyi, G. Nowaczyk, M. Jarek, E. Janiszewska, S. Jurga, ZnO size and shape effect on antibacterial activity and cytotoxicity profile, Sci. Rep. 12 (1) (2022) 8148.
[71] W. Yu, R. Liu, Y. Zhou, H. Gao, Size-tunable strategies for a tumor targeted drug delivery system, ACS Cent. Sci. 6 (2) (2020) 100–116.
[72] M.A. Subhan, S.S.K. Yalamarty, N. Filipczak, F. Parveen, V.P. Torchilin, Recent advances in tumor targeting via EPR effect for cancer treatment, J. Pers. Med. 11 (6) (2021) 571.
[73] W. Jia, Y. Wang, R. Liu, X. Yu, H. Gao, Shape transformable strategies for drug delivery, Adv. Funct. Mater. 31 (18) (2021) 2009765.
[74] T. Ahmad, M.A. Bustam, M. Irfan, M. Moniruzzaman, H.M.A. Asghar, S. Bhattacharjee, Green synthesis of stabilized spherical shaped gold nanoparticles using novel aqueous Elaeis guineensis (oil palm) leaves extract, J. Mol. Struct. 1159 (2018) 167–173.
[75] B.M. Haryadi, D. Hafner, I. Amin, R. Schubel, R. Jordan, G. Winter, J. Engert, Nonspherical nanoparticle shape stability is affected by complex manufacturing aspects: its implications for drug delivery and targeting, Adv. Healthc. Mater. 8 (18) (2019) 1900352.
[76] S. Honary, F. Zahir, Effect of zeta potential on the properties of nano-drug delivery systems-a review (Part 2), Trop. J. Pharm. Life Sci. 12 (2) (2013) 265–273.
[77] Q. Ta, J. Ting, S. Harwood, N. Browning, A. Simm, K. Ross, I. Olier, R. Al-Kassas, Chitosan nanoparticles for enhancing drugs and cosmetic components penetration through the skin, Eur. J. Pharm. Sci. 160 (2021) 105765.
[78] M.O. Durymanov, A.A. Rosenkranz, A.S. Sobolev, Current approaches for improving intratumoral accumulation and distribution of nanomedicines, Theranostics 5 (9) (2015) 1007.
[79] Q. Liu, J. Guan, L. Qin, X. Zhang, S. Mao, Physicochemical properties affecting the fate of nanoparticles in pulmonary drug delivery, Drug Discov. Today 25 (1) (2020) 150–159.
[80] S.J. Cao, S. Xu, H.M. Wang, Y. Ling, J. Dong, R.D. Xia, X.H. Sun, Nanoparticles: oral delivery for protein and peptide drugs, AAPS PharmSciTech 20 (2019) 1–11.
[81] J. Witten, T. Samad, K. Ribbeck, Selective permeability of mucus barriers, Curr. Opin. Biotechnol. 52 (2018) 124–133.
[82] B. Hu, Y. Wang, M. Xie, G. Hu, F. Ma, X. Zeng, Polymer nanoparticles composed with gallic acid grafted chitosan and bioactive peptides combined antioxidant, anticancer activities and improved delivery property for labile polyphenols, J. Funct. Foods 15 (2015) 593–603.
[83] J. Li, G.H. Shin, I.W. Lee, X. Chen, H.J. Park, Soluble starch formulated nanocomposite increases water solubility and stability of curcumin, Food Hydrocoll. 56 (2016) 41–49.
[84] A. Dube, J.A. Nicolazzo, I. Larson, Chitosan nanoparticles enhance the intestinal absorption of the green tea catechins (+)-catechin and (-)-epigallocatechin gallate, Eur. J. Pharm. Sci. 41 (2010) 219–225.
[85] A. Barras, A. Mezzetti, A. Richard, S. Lazzaroni, S. Roux, P. Melnyk, D. Betbeder, N. Monfilliette-Dupont, Formulation and characterization of polyphenol-loaded lipid nanocapsules, Int. J. Pharm. 379 (2009) 270–277.
[86] A.A. Yetisgin, S. Cetinel, M. Zuvin, A. Kosar, O. Kutlu, Therapeutic nanoparticles and their targeted delivery applications, Molecules (Basel, Switzerland) 25 (2020) 2193.
[87] M. Fathi, A. Martín, D.J. McClements, Nanoencapsulation of food ingredients using carbohydrate based delivery systems, Trends Food Sci. Technol. 39 (2014) 18–39.
[88] X. Huang, C.S. Brazel, On the importance and mechanisms of burst release in matrix-controlled drug delivery systems, J. Control. Release 73 (2001) 121–136.
[89] J. Siepmann, N.A. Peppas, Modeling of drug release from delivery systems based on hydroxypropyl methylcellulose (HPMC), Adv. Drug Deliv. Rev. 64 (2012) 163–174.

[90] S.A. Agnihotri, N.N. Mallikarjuna, T.M. Aminabhavi, Recent advances on chitosan-based micro- and nanoparticles in drug delivery, J. Control. Release 100 (2004) 5–28.
[91] N. Bhattarai, J. Gunn, M. Zhang, Chitosan-based hydrogels for controlled, localized drug delivery, Adv. Drug Deliv. Rev. 62 (2010) 83–99.
[92] W.B. Liechty, D.R. Kryscio, B.V. Slaughter, N.A. Peppas, Polymers for drug delivery systems, Annu. Rev. Chem. Biomol. Eng. 1 (2010) 149–173.
[93] A.A. Date, J. Hanes, L.M. Ensign, Nanoparticles for oral delivery: design, evaluation and state-of-the-art, J. Control. Release 240 (2016) 504–526.
[94] R.W. Korsmeyer, R. Gurny, E. Doelker, P. Buri, N.A. Peppas, Mechanisms of solute release from porous hydrophilic polymers, Int. J. Pharm. 15 (1983) 25–35.
[95] G. Son, B.J. Lee, C.W. Cho, Mechanisms of drug release from advanced drug formulations such as polymeric-based drug-delivery systems and lipid nanoparticles, J. Pharm. Investig. 47 (2017) 287–296.
[96] D.J. McClements, Encapsulation, protection, and delivery of bioactive proteins and peptides using nanoparticle and microparticle systems: a review, Adv. Colloid Interf. Sci. 253 (2018) 1–22.
[97] L.W. Foo, E. Salleh, S.N.H. Mamat, Extraction and qualitative analysis of Piper betle leaves for antimicrobial activities, Int. J. Eng. Technol. Sci. Res. 2 (2) (2015) 1–8.
[98] H.T. Van, N.T. Le, D.L. Nguyen, G.B. Tran, N.T.A. Huynh, H.S. Vo, V.H. Chu, H.A. V. Truong, Q.H. Nguyen, Chemical profile and antibacterial activity of acetone extract of *Homalomena cochinchinensis* Engl. (Araceae), Plant Sci. Today 8 (1) (2021) 58–65.
[99] C.E. Juneious, Molecular biological determination of PKC inhibitory effects of 1,2,3-propanetriol monoacetate produced from marine sponge-associated bacteria, in: 3rd International Conference on Clinical Microbiology & Microbial Genomics, Valencia, Spain, 2014.
[100] M. Agoramoorthy, V. Chandrasekaran, M.J.H. Venkatesalu, Antibacterial and antifungal activities of fatty acid methyl esters of the blind-your-eye mangrove from India, Braz. J. Microbiol. 38 (2007) 739–742.
[101] Y. Yu, P.H. Correll, J.P. Vanden Heuvel, Conjugated linoleic acid decreases production of pro-inflammatory products in macrophages: evidence for a PPAR gamma dependent mechanism, Biochim. Biophys. Acta 1581 (2002) 89–99.
[102] J.L. Lawrence, G.B. Eric, B.Z. Robert, Treatment of rheumatoid arthritis with gamma linolenic acid, Ann. Intern. Med. 119 (1993) 9.
[103] H.B. MacDonald, Conjugated linoleic acid and disease prevention: a review of current knowledge, J. Am. Coll. Nutr. 19 (2) (2000).
[104] Z. Chen, Q. Liu, Z. Zhao, B. Bai, Z. Sun, L. Cai, Y. Fu, Y. Ma, Q. Wang, G. Xi, Effect of hydroxyl on antioxidant properties of 2,3-dihydro-3,5-dihydroxy-6-methyl-4H-pyran-4-one [96to scavenge free radicals], RSC Adv. 11 (55) (2021) 34456–34461.
[105] S. Lalitha, B. Parthipan, V.R. Mohan, Determination of bioactive components of Psychotria nilgiriensis Deb & Gang (Rubiaceae) by GC-MS analysis, Int. J. Pharm. Phytochem Res. 7 (2015) 802–809.
[106] I. Platt, A. El-Sohemy, Effects of 9cis, 11trans and 10trans, 12cis CLA on osteoclast formation and activity from human CD14 + monocytes, Lipids Health Dis. 8 (1) (2009) 1–9.
[107] A.B. Hsouna, M. Trigie, R.B. Mansour, R.M. Jarraya, M. Damak, S. Jaoua, Chemical composition, cytotoxicity effect and antimicrobial activity of Ceratonia silisqua essential oil with preservative effects against Listeria inoculated in minced beef meat, Int. J. Food Microbiol. 148 (1) (2011) 66–72.
[108] S. Tricon, G.C. Burdge, S. Kew, T. Banerjee, J.J. Russell, E.L. Jones, R.F. Grimble, C.M. Williams, P. Yaqoob, P.C. Calder, Opposing effects of cis-9, trans-11 and trans-10, cis-12 conjugated linoleic acid on blood lipids in healthy humans, Am. J. Clin. Nutr. 80 (3) (2004) 614–620.
[109] I.H. Khan, A. Javaid, Anticancer, antimicrobial and antioxidant compounds of quinoa inflorescence, Adv. Life Sci. 8 (1) (2020) 68–72.
[110] S.B. Rao, C.P. Sharma, Use of chitosan as a biomaterial: studies on its safety and hemostatic potential, J. Biomed. Mater. Res. 34 (1997) 21–28.
[111] B.W. Neun, M.A. Dobrovolskaia, Method for analysis of nanoparticle hemolytic properties in vitro, Methods. Mol. Biol. (Clifton, N.J.) 697 (2011) 215–224.
[112] S. Rajeshwari, A.S. Biswas, J. Suresh, E. Alves, B.M. Gurupadayya, A. Pilli, S. V. Madhunapantula, P. Pattaluchetty, Phytochemicals from corn plant as anti-inflammatory agents: molecular insights and therapeutic perspectives, Pharmacological Research - Natural Products 1 (2026) 100497.
[113] G. Davidov-Pardo, D.J. McClements, Nutraceutical delivery systems: resveratrol encapsulation in grape seed oil nanoemulsions formed by spontaneous emulsification, Food Chem. 167 (2015) 205–212.
[114] T. Kean, M. Thanou, Biodegradation, biodistribution and toxicity of chitosan, Adv. Drug Deliv. Rev. 62 (2010) 3–11.
[115] F. Garavand, M. Jalai-Jivan, E. Assadpour, S.M. Jafari, Encapsulation of phenolic compounds within nano/microemulsion systems: a review, Food Chem. 364 (2021) 130376.
[116] T.M. Allen, P.R. Cullis, Liposomal drug delivery systems: from concept to clinical applications, Adv. Drug Deliv. Rev. 65 (2013) 36–48.
[117] J. Liu, C. Wang, Z. Wang, C. Zhang, S. Lu, J. Liu, The antioxidant and free-radical scavenging activities of extract and fractions from corn silk (Zea mays L.) and related §avone glycosides, Food Chem. 126 (1) (2011) 261–269.
[118] A.F. Naeimi, M. Alizadeh, Antioxidant properties of the flavonoid fisetin: an updated review of in vivo and in vitro studies, Trends Food Sci. Technol. 70 (2017) 34–44.
[119] Y. Jia, X. Gao, Z. Xue, Y. Wang, Y. Lu, M. Zhang, P. Panichayupakaranant, H. Chen, Characterization, antioxidant activities, and inhibition on α-glucosidase activity of corn silk polysaccharides obtained by different extraction methods, Int. J. Biol. Macromol. 163 (2020) 1640–1648.
[120] G.Q. Wang, T. Xu, X.M. Bu, B.Y. Liu, Anti-inflammation effects of corn silk in a rat model of carrageenan induced pleurisy, Inflammation 35 (2012) 822–827.
[121] S. Sarfare, S.I. Khan, F. Zulqar, S. Radhakrishnan, Z. Ali, I.A. Khan, Undescribed C-glycosylflavones from corn silk and potential anti-inflammatory activity evaluation of isolates, Planta Med. 88 (09/10) (2022) 745–752.
[122] Y. Li, Z. Hu, X. Wang, M. Wu, H. Zhou, Y. Zhang, Characterization of a polysaccharide with antioxidant and anti-cervical cancer potentials from the corn silk cultivated in Jilin province, Int. J. Biol. Macromol. 155 (2020) 1105–1113.
[123] K.K. Oh, M. Adnan, D.H. Cho, Elucidating drug-like compounds and potential mechanisms of corn silk (Stigma Maydis) against obesity: a network pharmacology study, Curr. Issues Mol. Biol. 43 (3) (2021) 1906–1936.
[124] B. Kumar, K. Jalodia, P. Kumar, H.K. Gautam, Recent advances in nanoparticle-mediated drug delivery, J. Drug Deliv. Technol. 41 (2017) 260–268.
[125] R. van der Meel, E. Sulheim, Y. Shi, F. Kiessling, W.J. Mulder, T. Lammers, Smart cancer nanomedicine, Nat. Nanotechnol. 14 (11) (2019) 1007–1017.
[126] A.F. Esfanjani, E. Assadpour, S.M. Jafari, Improving the bioavailability of phenolic compounds by loading them within lipid-based nanocarriers, Trends Food Sci. 76 (2018) 56–66.
[127] A. Shah, S. Aftab, J. Nisar, M.N. Ashiq, F.J. Iftikhar, Nanocarriers for targeted drug delivery, J. Drug Deliv. Technol. 62 (2021) 102426.
[128] C. Melim, M. Magalhães, A.C. Santos, E.J. Campos, C. Cabral, Nanoparticles as phytochemical carriers for cancer treatment: news of the last decade, Expert Opin. Drug Deliv. 19 (2) (2022) 179–197.
[129] M.A. Abdel-Wahhab, A. Aljawish, A.A. El-Nekeety, S.H. Abdel-Aziem, N. S. Hassan, Chitosan nanoparticles plus quercetin suppress the oxidative stress, modulate DNA fragmentation and gene expression in the kidney of rats fed ochratoxin A-contaminated diet, Food Chem. Toxicol. 99 (2017) 209–221.
[130] N.R. Mohamed, T.M. Badr, M.R. Elnagar, Efficiency of curcumin and chitosan nanoparticles against toxicity of potassium dichromate in male mice, Int J Pharm Pharm Sci 13 (2021) 22159.
[131] J.C. Antunes, T.D. Tavares, M.A. Teixeira, M.O. Teixeira, N.C. Homem, M.T. P. Amorim, H.P. Felgueiras, Eugenol-containing essential oils loaded onto chitosan/polyvinyl alcohol blended films and their ability to eradicate *Staphylococcus aureus* or *Pseudomonas aeruginosa* from infected microenvironments, Pharmaceutics 13 (2021) 195.
[132] A. Tawfik, A. Farid, Chitosan-encapsulated Aloe vera nanoparticles outperform carrier-free forms in enhancing MSCs therapy for amikacin nephrotoxicity, Sci. Rep. 15 (2025) 34292.